A Parametric Wave Prediction Model

K. HASSELMANN,[1] D. B. ROSS,[2] P. MÜLLER[3] AND W. SELL[1]

(Manuscript received 5 May 1975, in revised form 18 August 1975)

ABSTRACT

Measurements of fetch-limited wave spectra from various sources indicate an approximate invariance of the normalized spectral shape with fetch. It has been suggested from investigations of the spectral energy balance that this can be explained by the shape-stabilizing influence of nonlinear resonant wave-wave interactions, which are also responsible for the migration of the spectral peak to lower frequencies. Analyses of a series of further data sets obtained under non-uniform, non-stationary wind conditions show that the invariance of the spectral shape is not restricted to uniform-wind, fetch-limited situations, but applies generally for a growing wind sea. The observed shape invariance is exploited in a wave prediction model by projecting the full transport equation for the two-dimensional spectral continuum onto two variables characterizing the energy and frequency scales of the spectrum. Inspection of the resultant equations reveals further simplifications, enabling the system to be reduced to a single prediction equation for one scale variable, the peak frequency. This is feasible because of the rapid adjustment of the spectrum to a quasi-equilibrium level in which the atmospheric input is balanced by the nonlinear transfer of energy out of the central region of the spectrum to higher and lower frequencies. The balance occurs sufficiently rapidly to be treated as a local response process, thereby providing a relation between the energy level of the spectrum (characterized, for example, by Phillips' constant α), the peak frequency f_m, and the local wind speed U (the latter two occurring only in the non-dimensional combination $\nu = Uf_m/g$).

The directional distribution of the wave spectrum is also established locally and can be regarded as a given function of the non-dimensional frequency f/f_m and ν. For the remaining independent scale parameter, the peak frequency, the dominant source term in the transport equation is determined by the nonlinear energy transfer, which can be computed rigorously. To lowest order, the one-parameter wave model is independent of the relative contributions of the atmospheric input and dissipation in the central region of the spectrum. However, because of lack of (consistent) direct measurements of the atmospheric input or dissipation, the quasi-equilibrium relation inferred between α and ν must be calibrated empirically, for example, by comparison with fetch-limited data. Within the scatter of the data, all data sets analyzed (with two exceptions, where the data were considered questionable) were reasonably consistent with a common α–ν relation. The residual scatter of the data is thought to be associated largely with small (subgrid) scale inhomogeneities of the wind field and may represent a natural limitation of the accuracy achievable with deterministic wave models. A complete wave model would need to combine the proposed parametric model for growing wind seas with a swell propagation model.

1. Introduction

Numerical wave prediction models have traditionally been based on a synthesis of empirical wave-growth data, theories of wave dynamics, and hypotheses, where both theory and data are lacking. This approach will be needed as long as our knowledge of the principal processes controlling the energy balance of the surface-wave spectrum itself remains incomplete. However, it may be expected that the models will be successively improved as more data become available and a clearer picture of the structure of the spectral energy balance emerges. Since the development of the first generation of wave models based on the transport equation by Gelci *et al.* (1957), Pierson *et al.* (1966), Barnett (1968) and Ewing (1971) [see also the review by Gelci and Devillaz (1970)], many wave measurements have been made, including extensive wave-growth studies under well-defined wind conditions during the Joint North Sea Wave Project [JONSWAP, Hasselmann *et al.* (1973); referred to in the following as J]. These have clarified some of the principal mechanisms controlling the evolution of the wave spectrum, and the time therefore appears appropriate for a fresh look at the wave prediction problem.

The need for a modification of existing wave models is underscored by the basically different explanation of earlier wave-growth data resulting from the JONSWAP study as compared with the original interpretations on which these models were based. In the past, wave-growth data have normally been fitted with linear-exponential growth functions, in accordance with a combined Phillips-Miles generation mechanism (Snyder

[1] Max-Planck-Institute für Meteorologie, Hamburg.
[2] Sea-Air Interaction Laboratory, NOAA, Miami, Fla.
[3] Sonderforschungsbereich 94, Meeresforschung, University of Hamburg, and Max-Planck-Institut für Meteorologie.

and Cox, 1966; Barnett and Wilkerson, 1967). However, the atmospheric input into the wave field inferred in this manner was found to be considerably larger than, and therefore incompatible with, the known total momentum transfer across the air-sea interface (cf. Snyder and Cox, 1966). This paradox was resolved in J, where it was shown that the rapid growth of waves on the forward face of the spectrum was associated primarily with the nonlinear energy flux across the peak due to resonant wave-wave interactions (Hasselmann, 1962, 1963a,b). Moreover, it was found that the nonlinear energy transfer controlled not only the rate of growth of the newly developing waves, but also the form of the spectrum, in particular the development of a pronounced peak, and the migration of the peak toward lower frequencies. Atmospheric forcing has little direct influence on these processes and is important only in determining the overall level which the spectrum attains until the atmospheric input in the central region of the spectrum can be balanced by the nonlinear energy transfer out of this region to lower and higher frequencies.

With regard to wave prediction, these findings are significant not only for the proper description of the source function in the transport equation, but also for the choice of appropriate numerical techniques. As soon as the nonlinear transfer becomes a non-negligible term in the energy balance, some form of parameterization of the spectrum becomes necessary, since the exact evaluation of the Boltzmann integrals describing the nonlinear interaction rates far exceeds the time available for numerical integration of the transport equation. In previous prediction models, the nonlinear resonant transfer terms were either ignored entirely (e.g., Gelci *et al.*, 1957; Pierson *et al.*, 1966) or were parameterized in a rather simple manner (cf. Barnett, 1968; Ewing, 1971). The remaining propagation, input and dissipation terms, all of which were normally regarded as decoupled processes with respect to wavenumber, were then treated numerically by the standard procedure of discretizing the two-dimensional wavenumber (or frequency-direction) spectrum. However, to the extent that the nonlinear energy transfer turns out to be a controlling process in the overall energy balance, there appears little point in describing the remaining terms in the transport equation—or the spectrum itself—in greater detail than the nonlinear terms. Accordingly, we shall consider in the following a parametric wave model in which the complete transport equation in the frequency-direction domain is projected onto the very much smaller parameter space used to represent the nonlinear energy transfer. A general projection technique is described in J. We shall be concerned here with a simple version of the general procedure which is based on the observation that for growing seas all wave spectra appear to have a rather similar shape. It is found that the average shape of underdeveloped spectra measured by different authors under a wide variety of conditions corresponds fairly closely to the mean JONSWAP spectrum. Assuming that this similarity also applies to the directional distributions, the parameter space needed to describe the properties of a growing wave spectrum can be reduced to only two parameters defining the energy and frequency scales of the one-dimensional spectrum. The nonlinear terms in the resulting parametric transport equations can be computed rigorously; the remaining terms can then be obtained by calibration against the JONSWAP data. To close the problem, it is assumed first that the atmospheric input is linear with respect to the wave spectrum and that dissipation, although important as a high-wavenumber sink, is negligible in the main part of the spectrum.

Investigation of the transport equations reveals that for normal (not excessively variable) wind fields all solutions lie rather close to a single curve in the parameter plane. This implies that the two scale parameters are related, and the prediction problem can be reduced still further to the determination of a single wave parameter, e.g., the peak frequency.

Physically, the description of the wave field in terms of only two scale parameters is possible because of the stabilizing effect of the nonlinear interaction on the spectral shape (cf. J) and the further reduction to a single parameter because of the rapid adjustment of the spectrum to a quasi-equilibrium level at which the atmospheric input in the central region of the spectrum is balanced by the nonlinear energy transfer. However, across the peak the nonlinear source function changes very rapidly from positive to negative values and is unable to balance the positive, more smoothly varying source function for the atmospheric input. The imbalance in this narrow frequency band results in the migration of the peak, and the prediction problem reduces essentially to the determination of this rate of shift. For the one-parameter approximation it is irrelevant whether or not dissipation contributes to the energy balance in the central region of the spectrum, provided that the sum of input plus dissipation, which together must balance the nonlinear transfer, is tuned such that the equilibrium level observed in the fetch-limited studies is correctly predicted, since the shift of the peak is controlled entirely by the known nonlinear transfer. Fortunately, therefore, the present ignorance of the structure of the input and dissipation source functions is not critical for the model.

Measurements of growing waves collected from widely differing sources are found to cluster fairly well along the predicted universal curve in the two-parameter phase plane. However, the proposed simple prediction model should be regarded only as a first approximation to more sophisticated models containing a larger number of parameters. The approximation assumes that the characteristic relaxation times associated with the shape stabilization and energy-level equilibrium are

small compared with other time scales, such as the propagation time of the waves through the wind field. While the wave data presented below for growing and nearly fully developed wave spectra appear to support this assumption, there also exist cases in which the approximation is clearly invalid.

An obvious example is swell. Here the atmospheric input needed to support the spectrum at a level at which the nonlinear interactions become effective is lacking, and the wave energy is accordingly reduced so far that the individual wave components are dynamically almost completely decoupled. Thus in contrast to the wind-sea model, the shape of a swell spectrum is not universal but depends on the details of the time, position and extent of the wave source. The superposition of swell, which is nearly always present in the ocean, on a developing wind sea should not affect the application of the model to the wind-sea region of the spectrum, since resonant nonlinear interactions between swell and wind sea are extremely weak (Hasselmann, 1963b). In principle, swell and wind sea can interact also through WKB-type (radiation stress) interactions (cf. Phillips, 1963; Longuet-Higgins and Stewart, 1964; Hasselmann, 1971) but attempts to discover this effect in field experiments have so far been unsuccessful [Snodgrass *et al.*, 1966; J—see however Mitsuyasu (1966) and Reece and Shemdin (1974) who have found an influence of longer gravity waves on shorter wind-generated waves in a wind-wave tank]. The field evidence indicates that well-dispersed swell can be regarded as decoupled from the wind-sea components considered in our model.

However, there also exist less obvious transitions between wind sea and swell where the assumption of a universal spectral shape will presumably break down. Examples are rapidly turning winds, such as in fronts, producing cross seas of comparable frequency, or the rebirth of a swell field as a wind sea in a freshening wind situation, when the wind speed parallel to the direction of propagation of the waves begins to exceed the swell phase speed. In the latter case the wind-sea spectrum will generally contain two peaks, the normal high-frequency wind-sea peak and the former swell peak. As the low-frequency peak begins to gain energy under the influence of the wind, the two peaks will begin to interact nonlinearly and the spectrum will presumably readjust to the universal equilibrium form. However, the relaxation time depends on the separation of the peaks and will generally be larger than the relaxation time for the redistribution of energy within a peak. A general wave-prediction model will probably need to combine a more sophisticated multi-parametric treatment of the wind-sea region of the spectrum, including multiple peaks, with a traditional characteristic method of swell prediction. The simple model presented here may nevertheless be adequate for many applications in which the detailed structure of the spectrum is not too critical; an example involves the computation of wave-climate statistics from existing wind-field statistics.

2. The shape-invariance of wind-sea spectra

Nearly all fetch-limited frequency spectra measured during JONSWAP could be fitted closely with a function of the general form

$$E(f)=\alpha g^2(2\pi)^{-4}f^{-5}\exp\left\{-\frac{5}{4}\left(\frac{f_m}{f}\right)^4+\ln\gamma\right.$$
$$\left.\times\exp\left[-\frac{(f-f_m)^2}{2\sigma^2 f_m^2}\right]\right\}, \quad (2.1)$$

where

$$\sigma=\begin{cases}\sigma_a, & f\leqslant f_m\\ \sigma_b, & f\geqslant f_m\end{cases}.$$

The function contains five free parameters, two scale parameters (f_m the frequency of the spectral peak and α Phillips constant) and three shape parameters (the peak-enhancement factor γ which is ratio of the peak value of the spectrum to the peak value of the corresponding Pierson-Moskowitz spectrum with the same values of f_m and α, σ_a the left peak width, and σ_b the right peak width). The form (2.1) is derived from the Pierson-Moskowitz (PM) (1964) fully developed spectrum by multiplying with the peak-enhancement function

$$\gamma\exp\left[\frac{-(f-f_m)^2}{2\sigma^2 f_m^2}\right].$$

It reduces to the PM spectral shape for $\gamma=1$. The scale parameters for the PM spectrum itself have the fixed values $\alpha=0.0081$,

$$f_m=\left(\frac{0.74}{1.25}\right)^4 g/(2\pi U)=0.14\ g/U,$$

where U is the wind speed (defined by Pierson and Moskowitz as the 19.5 m anemometer height wind, but we shall refer all winds in the following to an anemometer height of 10 m).

It has been pointed out by Kitaigorodskii (1962), for the simple geometry of a uniform, stationary wind blowing perpendicularly off a straight shore line, that all wave field variables, when non-dimensionalized in terms of g and U, should be functions only of the single non-dimensional variable $\xi=gx/U^2$. Both field and laboratory data conform fairly well with Kitaigorodskii's scaling relation over a wide range of non-dimensional fetches (cf. J). The possible influence on wave growth of other external parameters such as the air-sea temperature difference and local currents has often been discussed, but attempts to find such correlations within the range of external conditions encountered during JONSWAP were unsuccessful.

Over the non-dimensional fetch range $10^{-1}<\xi<10^4$, encompassing both wind-wave tank data ($10^{-1}<\xi<10^1$) and field data ($10^2<\xi<10^4$) from many sources, the

fetch dependence of the non-dimensional peak frequency $\nu = Uf_m/g$ and α can be described fairly well by the power-law relations (J)

$$\nu = 3.5\ \xi^{-0.33}, \tag{2.2}$$

$$\alpha = 0.076\ \xi^{-0.22}. \tag{2.3}$$

It will be found useful to consider also the variance of the surface displacement $\mathcal{E} = \int E(f)df$, or its nondimensional form $\epsilon = \mathcal{E}g^2/U^4$, as an alternative scale parameter. In the same fetch range this shows a linear fetch dependence, i.e.,

$$\epsilon = 1.6 \times 10^{-7}\ \xi. \tag{2.4}$$

Power laws very similar to (2.2), (2.3) or (2.4) have been proposed also by other works (cf. Mitsuyasu, 1968, 1969, 1973; Wilson, 1965). The western Atlantic data set can also be examined in this manner and yields $\nu \propto \xi^{-0.27}$ and $\epsilon \propto \xi^{1.1}$. The Phillips parameter α, however, showed little fetch dependence for the rather large fetch present. The shape parameters γ, σ_a and σ_b exhibited appreciable scatter, but no significant mean dependence on fetch. An alternative shape parameter which depends on average spectral properties and is thus less affected by individual variations of the peak shape parameters may be defined as $\lambda = \epsilon\nu^4/\alpha$. The relations (2.2), (2.3) and (2.4) imply $\lambda \sim \xi^{-0.1}$, but this weak fetch dependence is not discernible within the scatter of the JONSWAP data.

The mean shape of the JONSWAP spectra agrees well with the shape of other fetch-limited spectra measured (e.g., Barnett and Wilkerson, 1967; Mitsuyasu, 1968, 1969, 1973; Ross *et al.*, 1970; Ross and Cardone, 1974; Schule *et al.*, 1971). The same shape has also been observed in wind-wave tank experiments (e.g., Mitsuyasu, 1968, 1969). Recently, Snyder (1974) has found that the form (2.1) [with $\sigma_a = \sigma_b$] gives good fits to his spectra measured in the Bight of Abaco and to spectra observed by Elliott (1972) and Dobson (1971) on the Spanish Banks, Vancouver. Liu's (1971) spectra in Lake Michigan also correspond to the form (2.1). These spectra were all obtained under stationary, fetch-limited conditions, but in most cases for winds that were not perpendicularly offshore. To compare with these measurements, we have analyzed a number of additional JONSWAP spectra for non-perpendicular offshore winds; they could again be fitted satisfactorily with the function (2.1).

An equally good fit is found for growing wind-sea (duration-limited) spectra measured away from limiting boundaries. These include high wind spectra measured by shipborne wave recorders of the UK weather ships *Weather Explorer* and *Weather Reporter*, and from the U. S. Navy Argus Island research platform (Pickett, 1962; Manasseri, 1967; DeLeonibus *et al.*, 1974). A good fit was also obtained for wave data measured by one of us during Pacific hurricane Ava in 1973, and by the oil industry during hurricane Camille (Patterson, 1974). Good agreement in the case of the hurricanes is especially notable considering the moving, circular nature of a hurricane wind field. Some examples of the above spectral fits are given in Fig. 1.

A summary of the shape variables for typical sets of field measurements is given in Table 1. Also shown are the corresponding values for a composite data set consisting of a superposition of all data with the exception of the sets marked with an asterisk (which are discussed below). (The last two column groups in the table refer to the energy-scale variables α and ϵ, which will be discussed in Section 10.) For each data set the dependence of the shape parameters $s = \gamma, \sigma_a, \sigma_b, \lambda$ on the state of development of the wave field was investigated by fitting least-square regression lines

$$\log s = r(\log\nu - \log\nu_0) + \log s_0$$

through plots of $\log s$ versus the logarithm of the nondimensional frequency ν. The reference frequency $\nu_0 = 0.251$ ($\log\nu_0 = -0.60$) was defined as the mean of $\log\nu$ over all data sets; the regression line then determines the exponent r and factor s_0 for a power law fit $s = s_0(\nu/\nu_0)^r$ for each shape parameter s. The uncertainty intervals represent the standard deviations in the determination of the regression line parameters from a finite sample size (cf. Jenkins and Watts, 1969). The standard deviations listed separately in the table refer to the rms deviation of individual values of $\log s$ from the regression line, expressed in equivalent percentage variations of s. Winds used in the calculations of dimensionless parameters were either measured at 10 m, or adjusted to this height using the technique suggested by Cardone (1969).

Plots of γ and λ for the composite data set are shown in Figs. 2 and 3. The statistical uncertainty of the regression line is indicated by two hyperbolas representing the envelopes of the family of lines obtained by varying s_0 and r between limits set by their standard deviations. Note that the peak enhancement factor γ (as all shape parameters dependent primarily on the shape of the peak) is more strongly scattered than the integral shape parameter λ. The standard deviations listed in Table 1 indicate that the scatter for the composite data set is not significantly greater than for individual subsets, including highly filtered data such as set A, which is restricted to stationary, uniform, orthogonally offshore wind fields. Inspection of individual generation cases for this data set suggests that the scatter is not due to hidden external parameters but is associated with small (subgrid) scale inhomogeneities of the wind field (cf. J). Table 1 and Figs. 2, 3 show no systematic dependence of the shape parameters on the state of development of the spectrum, although for data sets D and F the regression lines do suggest decreasing peak-enhancement factors as one approaches the limiting frequency $\nu = 0.14$ for a fully developed (Pierson-Moskowitz) spectrum. However, these data are limited to a rather

narrow ν range and the slopes of the lines are not well determined.

The mean values of all shape parameters listed in Table 1 do not differ appreciably from the mean JONSWAP values

$$\gamma=3.3, \quad \sigma_a=0.07, \quad \sigma_b=0.09, \quad \lambda=1.6\times10^{-4}.$$

We shall adopt these values in the following in order to make use of the nonlinear energy transfer calculations which were carried out for the mean JONSWAP spectrum in J.

Data sets E, H and I were excluded from the composite data set. The *Weather Adviser* spectra E yield very small γ values. These might be attributed to rather high values of α (cf. Section 10). We can offer no obvious explanation for this discrepancy (apart from possible calibration problems of the shipborne wave recorder at high frequencies), but the data appear somewhat questionable and were therefore discarded. Anomalous α values were also found for the short fetch data H obtained for the Spanish Banks and the Bight of Abaco. The α values for the Spanish Banks were highly

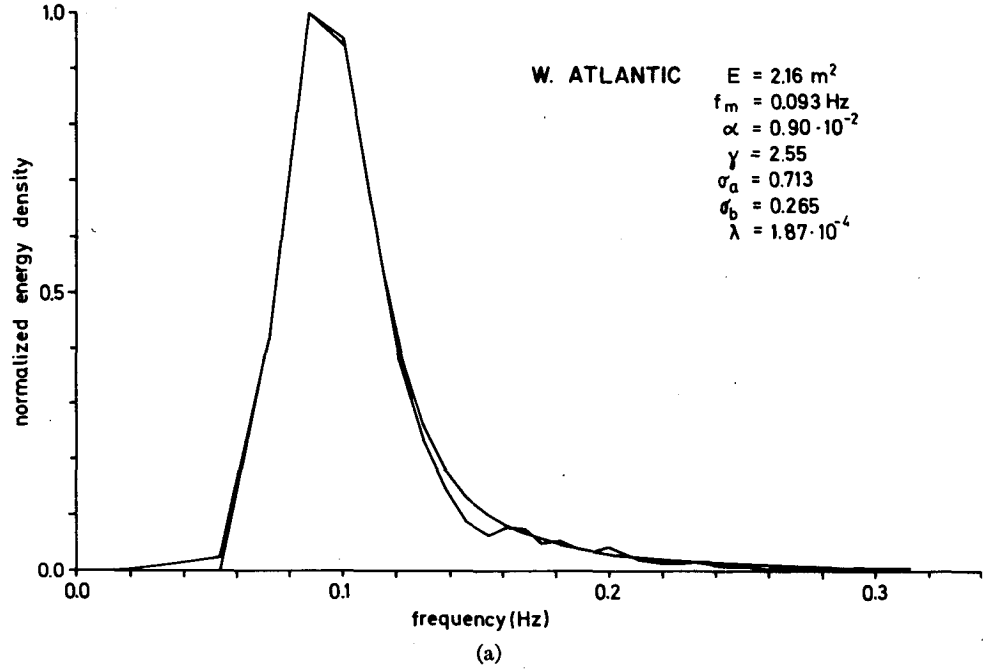

(a)

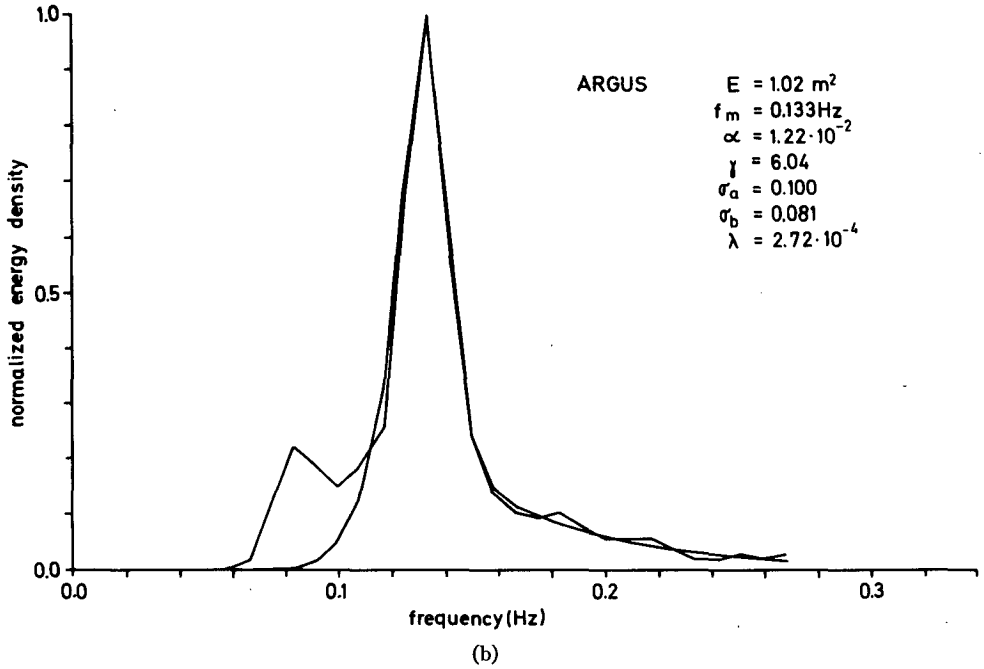

(b)

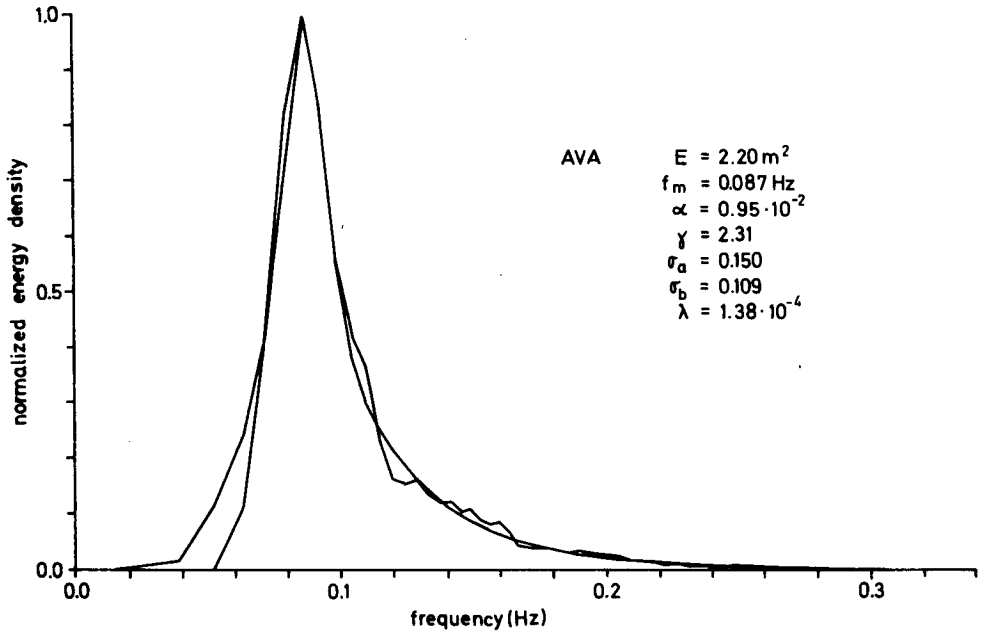

(c)

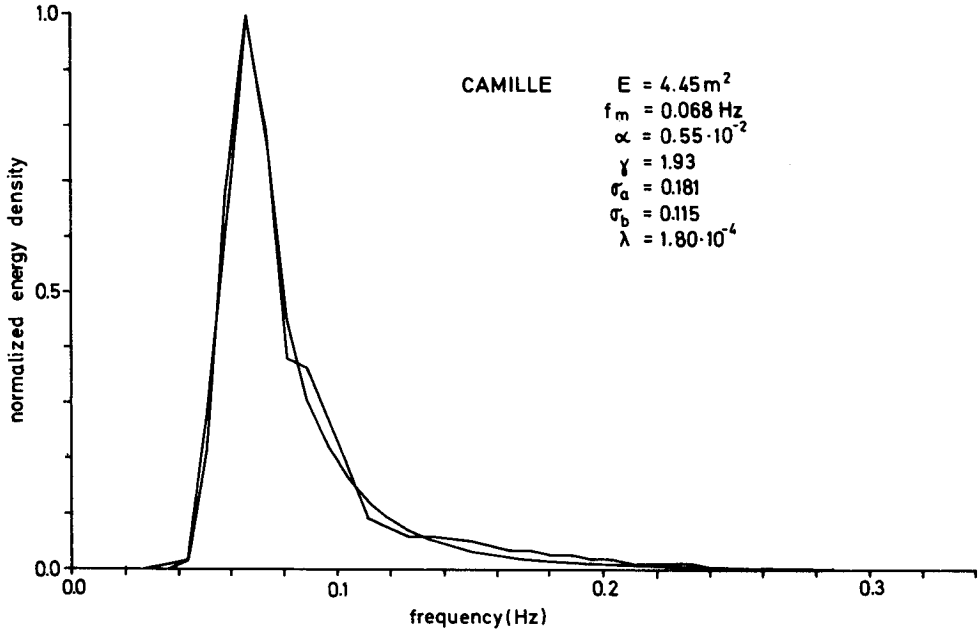

(d)

FIG. 1. Examples of spectra and analytical fits for data sets B (western Atlantic), F (Argus Island) and G (hurricanes Ava and Camille), (a)–(d), respectively.

scattered (possibly due to refraction by currents, which is particularly effective for short waves), and the Bight of Abaco α data were anomalously low (cf. Section 10). Although the data were excluded for these reasons from the composite data set, the shape parameters themselves do not in fact show any anomalies compared with the other data.

The spectral set I deserves special mention. It is a subset of the spectra used by Pierson and Moskowitz (1964) to derive their formula for the fully developed spectrum. Since the JONSWAP and other fetch-limited spectra showed no marked decrease of γ toward 1 with increasing fetch, as to be expected if the spectra approach the fully developed Pierson-Moskowitz form for large ξ, the Pierson-Moskowitz spectral set was reanalyzed using the same parameter-fitting scheme as ap-

TABLE 1. Regression line variables of shape and scale parameters.

Data set	Source	Description	Number of spectra	γ			σ_a			σ_b			λ			α			ϵ		
				γ_0	r	S.D. (%)	$\sigma_{a0}\times10^2$	r	S.D. (%)	$\sigma_{b0}\times10^2$	r	S.D. (%)	$\lambda_0\times10^4$	r	S.D. (%)	$\alpha_0\times10^2$	r	S.D. (%)	$\epsilon_0\times10^4$	r	S.D. (%)
A	Hasselmann *et al.* (1973)	JONSWAP, North Sea, orthogonal fetch	121	3.43 ±0.14	−0.16 ±0.08	29	(9.12 ±0.69)	−0.34 ±0.16	55	(9.54 ±0.47	−0.04 ±0.10	36	(2.04 ±0.05	−0.12 ±0.05	19	1.00 ±0.05	1.17 ±0.11	38.2	5.13 ±0.22	−2.95 ±0.09	32.2
B	Ross *et al.* (1970)	Western Atlantic, orthogonal fetch	25	3.81 ±0. 4	0.74 ±0.28	32	12.4 ±3.1	−1.65 ±0.63	71	11.7 ±1.4	−0.33 ±0.30	34	1.78 ±0.14	0.07 ±0.20	22	1.09 ±0.05	0.03 ±0.12	13.5	5.01 ±0.30	−3.90 ±0.15	17.2
C	Hasselmann *et al.* (1973)	JONSWAP, North Sea, slanting fetch	10	2.43 ±0.12	−0.07 ±0.18	48	6.02 ±0.61	0.36 ±0.36	84	8.71 ±0.62	−0.24 ±0.25	58	1.62 ±0.50	−0.03 ±0.11	30	0.93 ±0.03	0.980 ±0.14	36.2	3.89 ±0.15	−3.05 ±0.15	39.4
D	Moskowitz *et al.* (1962) Moskowitz *et al.* (1963)	Atlantic weather ships	49	4.20 ±0.71	1.83 ±0.40	40							3.09 ±0.38	1.10 ±0.29	29	0.95 ±0.15	0.48 ±0.39	38.0	7.24 ±1.06	2.42 ±0.35	34.5
E*	Snider and Chakrabarti (1973); Chakrabarti and Snider (1974)	Atlantic weather ship *Weather Adviser*	14	0.92 ±0.18	−0.03 ±0.53	36							1.05 ±0.09	−0.44 ±0.25	17	2.56 ±0.38	2.05 ±0.41	27.6	6.75 ±0.80	−1.99 ±0.33	22.4
F	DeLeonibus *et al.* (1974); Picket (1962); Manasseri (1967)	Argus Island	17	5.06 ±1.11	2.50 ±0.52	35	13.2 ±5.2	1.40 ±1.11	59	9.33 ±3.93	0.43 ±1.16	63	2.62 ±0.41	1.30 ±0.36	24	1.44 ±0.21	0.71 ±0.35	23.2	9.55 ±0.75	−2.00 ±0.18	12.3
G	Ross and Cardone (1974); Patterson (1974)	High winds (hurricanes Ava, Camille and North Sea storm)	20	2.67 ±0.52	0.09 ±0.76	64	10.4 ±2.9	−1.52 ±1.18	55	14.1 ±2.1	−0.11 ±0.55	48	1.70 ±0.15	0.14 ±0.34	29	1.29 ±0.13	1.29 ±0.40	33.8	5.37 ±0.78	−2.58 ±0.56	46.5
H*	Dobson (1971); Elliott (1972); Garrett (1969); Snyder (1974)	Spanish Banks, Vancouver Bight of Abaco (low waves)		2.69 ±0.18	0.14 ±0.19	19							2.57 ±0.36	0.38 ±0.36	33	0.62 ±0.11	0.48 ±0.42	61.9	3.89 ±1.17	−4.34 ±0.80	108.0
I*	Moskowitz (1963)	Atlantic weather ships, fully developed		3.91 ±3.18	1.49 ±1.07	62							3.39 ±1.72	1.09 ±0.70	40	2.95 ±1.95	2.16 ±0.89	51.5	25.11 ±11.41	−0.76 ±0.63	35.6
J		All data except sets E, H and I	333	2.65 ±0.06	0.32 ±0.06	44	8.51 ±0.44	−0.32 ±0.13	76	9.77 ±0.31	−0.16 ±0.08	47	1.82 ±0.27	0.08 ±0.04	28	1.09 ±0.02	0.87 ±0.05	38.6	5.01 ±0.11	−3.05 ±0.05	39.4

* Excluded sets (see text for discussion).

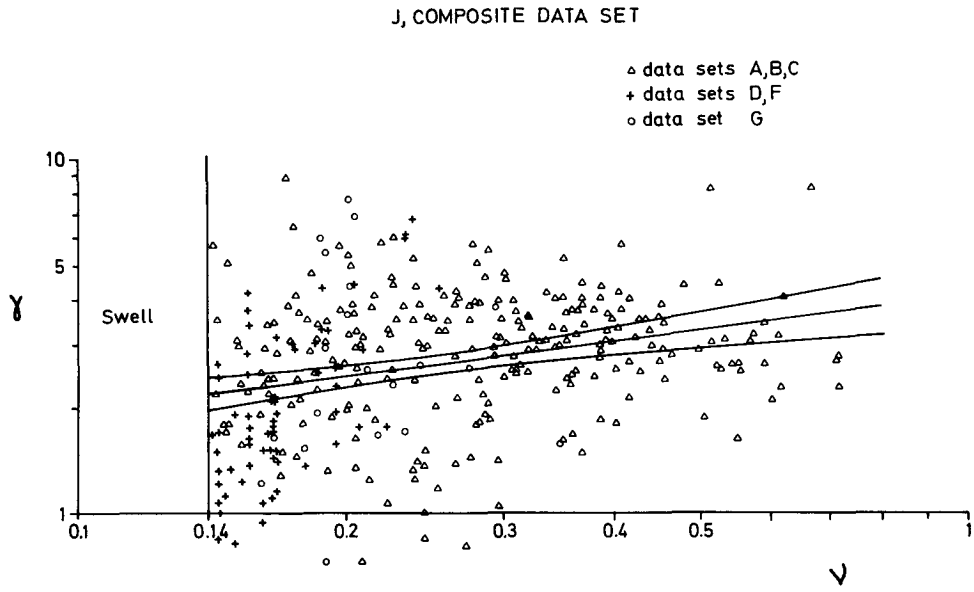

FIG. 2. Peak enhancement factor γ versus non-dimensional peak frequency $\nu = f_m U/g$ for the composite data set J.

plied to the JONSWAP and other spectra. Inspection of the PM spectra revealed that a little more than half contained multiple peaks, particularly for low wind speeds. Although the weather maps for these cases indicated uniform, stationary wind fields, we suspect that possibly they were in fact generated by weakly variable wind fields and represented transitional development stages of wind sea and swell. Multiple-peak spectra were accordingly excluded from the analysis. The remaining spectra yielded a mean peak-enhancement factor $\gamma = 1.40$. It should be pointed out that the Pierson-Moskowitz mean spectrum was obtained by superimposing all spectra within a given wind-speed interval (2.5 m s^{-1}), which tends to smooth individual peaks, whereas we have averaged the shape parameters as determined from the individual fits for each spectrum. Thus the "shape of the average spectrum," as considered by Pierson and Moskowitz, might be expected to differ from the "average shape of the spectrum," as considered here. The fact that both the Pierson-Moskowitz and our average γ value agree rather closely supports the conclusion that a fully developed spectrum is indeed considerably flatter than a growing wave spectrum, and that this feature is not an artifice of the particular averaging technique applied. Since we shall be concerned here with growing rather than fully developed seas, the set I was also excluded.

The fact that most fetch-limited studies yield γ values considerably higher than 1 for values of ν only slightly higher than the fully developed Pierson-

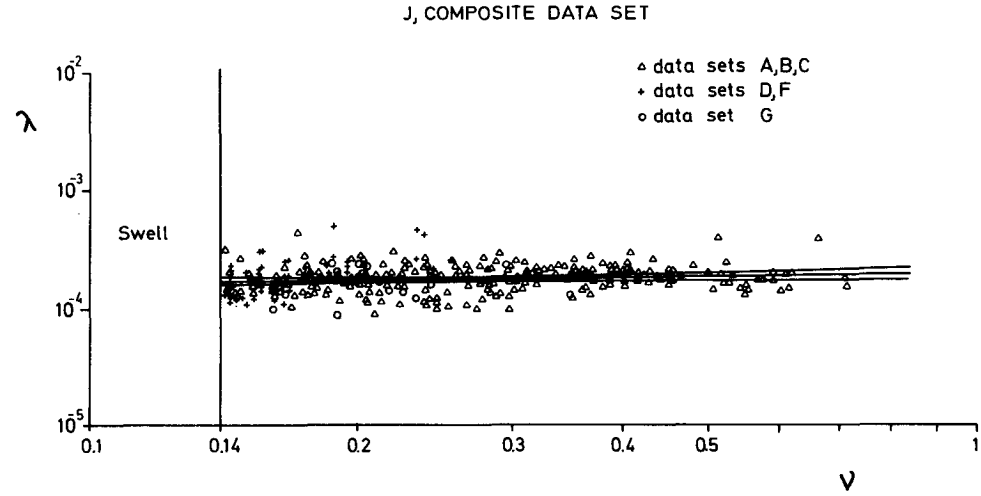

FIG. 3. Shape parameter λ versus non-dimensional peak frequency $\nu = f_m U/g$ for the composite data set J.

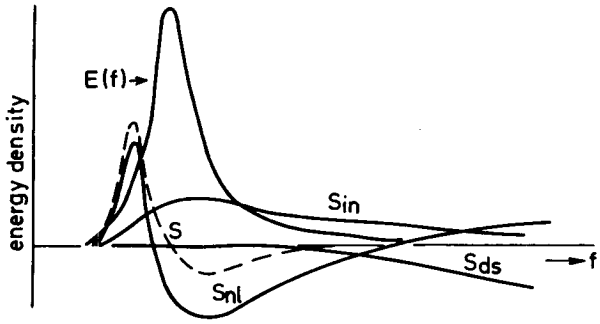

FIG. 4a. Structure of spectral energy balance for the case of a minimal input into the wave field. The dissipation is negligible for $f<2f_m$ (see Fig. 2.22 in JONSWAP).

Moskowitz value ($\nu=0.14$) indicates that the transition to the fully developed spectrum occurs in the very final stages of development. The transition process is not included in the simple constant-shape wave model considered in the following. A modification of the model to allow for this effect is basically straightfoward. (Qualitatively, the peak flattening can be readily explained in terms of the shape dependence of the nonlinear energy transfer and the decrease of the atmospheric input in the peak of the spectrum as the fully developed state is approached.) However, in practice, this shortcoming of the constant-shape model may not be serious, since the transition to the fully developed state apparently occurs very gradually and in a very late development stage. In most cases, particularly for high winds, the extent and duration of the uniform-wind region is insufficient to achieve a fully developed state, and the waves are transformed directly from an underdeveloped state into swell as the wind decays or the waves propagate out of the generation region (see also Section 9).

3. The spectral energy balance

From the JONSWAP data, it was inferred that the general form of the energy balance of the fetch-limited wave spectrum must lie somewhere between the two limiting cases shown in Fig. 4. Here S denotes the net source function of the one-dimensional transport equation

$$\frac{\partial}{\partial t}E(f)+\bar{v}\frac{\partial}{\partial x}E(f)=S, \tag{3.1}$$

obtained by integrating the two-dimensional transport equation

$$\frac{\partial}{\partial t}F(f,\theta)+v_k\frac{\partial}{\partial x_k}F(f,\theta)=T \tag{3.2}$$

over the propagation direction θ; and where

$$E(f)=\int F(f,\theta)d\theta,$$

$$\bar{v}=\int v_1F(f,\theta)d\theta/E(f)$$

is the directionally averaged group velocity in the x_1 direction parallel to the wind, and

$$S=\int Td\theta.$$

The other source functions in the figures represent the three individual constituents of the net source function,

$$S=S_{in}+S_{nl}+S_{ds}, \tag{3.3}$$

where S_{in} denotes the input from the atmosphere, S_{nl}

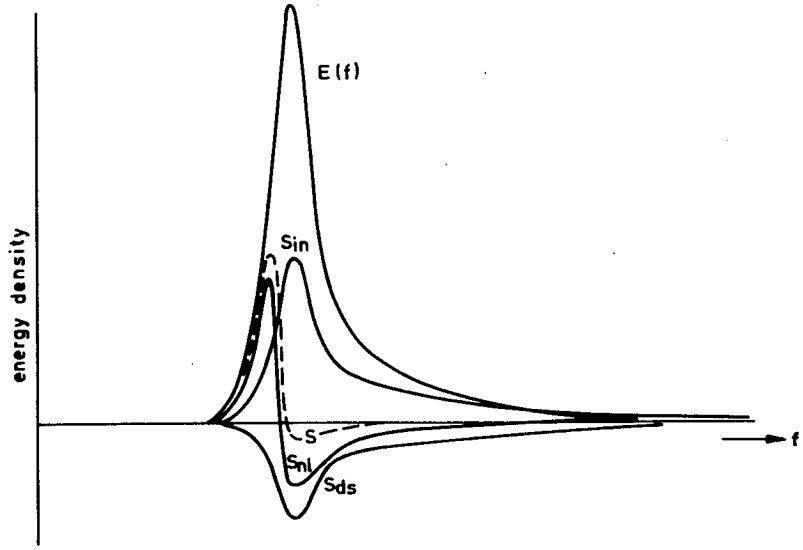

FIG. 4b. As in Fig. 4a except for a maximal input. The dissipation is in accordance with the white-capping model of Hasselman (1974, cf. Fig. 2).

the nonlinear energy transfer due to conservative wave-wave interactions, and S_{ds} the energy loss due to dissipative processes (including non-conservative nonlinear interactions associated, for example, with wave breaking or WKB-type interactions).

Of the four source functions S, S_{in}, S_{nl}, S_{ds}, the net source function S can be measured directly through the left-hand side of (3.1), and the nonlinear source function S_{nl} can be computed, leaving two unknown terms S_{in}, S_{ds} related by only one equation [(3.3)]. In principle, the input S_{in} can be determined directly through simultaneous measurement of the surface pressure and surface displacement, which yields the work done by the wind pressure forces against the waves. However, such experiments have not yet been made simultaneously with wave growth studies, and existing results from different workers (Dobson, 1971; Elliott, 1972; Snyder, 1974) are difficult to reconcile. Dobson found that essentially all of the momentum transfer across the air-sea interface goes into the waves, Elliott obtained a value of about 0.5 for the ratio of the wave-induced momentum transfer τ_w to the total transfer τ, and Snyder finds the far smaller ratio 0.02. Thus in the present situation the complete energy balance cannot be inferred from wave-growth studies without further assumptions regarding S_{in} or S_{ds}.

Fig. 4a represents qualitatively the form of the energy balance which results if one chooses S_{in} as small as possible, i.e., if the wave-induced drag coefficient $c_w=\tau_w/\delta_a U^2$ is a minimum consistent with the given functions S and S_{nl} (cf. J). The dissipation is taken as zero everywhere except at high frequencies, where a sink is needed to balance the positive nonlinear transfer. In the central part of the spectrum the energy losses associated with the negative lobe of S_{nl} are balanced by the atmospheric input S_{in}. It is assumed that the input is small in other regions of the spectrum, but positive. It is also assumed that the central region of the spectrum receives no energy from the short-wave region of the spectrum through WKB-type interactions. If the modulation of short waves by long waves is such that the short-wave energy is largest on the forward side of the long waves, as generally assumed, the direction of energy transfer for these interactions is from long waves to short waves (Hasselmann, 1971). Thus, if anything, these interactions would require a larger input to balance the losses in the central region of the spectrum, and it is consistent to ignore them in considering the minimum input energy balance. Applied to the JONSWAP data, the energy balance of Fig. 4a corresponds to $c_w\approx 0.2\times 10^{-3}$ for moderate to large fetches, $\xi=10^3-10^4$, and $c_w\approx 10^{-3}$ for small fetches ($\xi\approx 10^2$).

Fig. 4b represents the alternative limiting case in which all of the momentum transfer across the air-sea interface is wave-induced ($c_w\approx 10^{-3}$) at all fetches. In this case the increased input in the central region of the spectrum for moderate and larger fetches must be balanced by dissipation. [The distribution of S_{ds} shown in the figure corresponds to the particular form $S_{ds}=-\text{constant}\times f^2E$ derived for a white-capping model (cf. Hasselmann (1974).]

In both cases (Figs. 4a and 4b), the shape of the spectrum is independent of the detailed distribution of the input and dissipation functions, and is controlled primarily by the nonlinear energy transfer. Computations of the nonlinear energy transfer for various spectral shapes (J; Sell and Hasselmann, 1972) show that for a spectrum which is less sharply peaked than the mean JONSWAP spectrum the low-frequency positive lobe of S_{nl} shifts from the forward face of the spectrum to a position immediately below the peak, causing the peak to grow. Alternatively, if the peak becomes narrower than shown in Fig. 4b, the nonlinear source function S_{nl} develops an additional narrow positive lobe immediately to the right of the peak, and the peak broadens again. Thus, the spectrum adjusts to a self-stabilizing form which is continually maintained by the nonlinear transfer.

For the minimal input case, most of the momentum input τ_w to the waves is balanced by the nonlinear momentum transfer τ_{hf} into the positive, high-frequency lobe of S_{nl}. For a self-similar spectrum this scales as

$$\tau_{hf}=\text{constant}\times\rho_w\alpha^3 f_m^{-2}g^2,$$

or, in terms of a drag coefficient, as

$$c_{hf}=\frac{\tau_{hf}}{\rho_a U^2}=A\alpha^3\nu^{-2}. \tag{3.4}$$

For the mean JONSWAP spectrum, computations yield $A=3.6$ (cf. J).

The power laws (2.2) and (2.3) for α and ν correspond to a fetch-independent drag coefficient $c_{hf}=0.13\times 10^{-3}$. Adding to this the momentum stored in the wave field and advected away, which accounts for about 5% of total momentum transfer across the sea surface, one obtains a net wave-induced drag coefficient $c_w\approx 0.2\times 10^{-3}$, as quoted above for medium and large fetches. The larger JONSWAP values $c_w\approx 10^{-3}$ for small fetch are due to α values higher than the mean power law (2.3) in this range. However, taking all fetch-limited data from both wind-wave tank and field experiments in the range $10^{-1}<\xi<10^4$ into account, one finds an average value of $c_{hf}\approx 0.1-0.2\times 10^{-3}$.

For constant c_{hf} (and given spectral shape) Eq. (3.4) implies generally

$$\alpha=\left(\frac{0.13\times 10^{-3}}{A}\right)^{\frac{1}{3}}\nu^{\frac{2}{3}}=0.033\nu^{\frac{2}{3}}. \tag{3.5}$$

Expressed in terms of the nondimensional energy, $\epsilon=\mathfrak{F}g^2/U^4$, in place of α, where $\epsilon\nu^4/\alpha=\lambda=1.6\times 10^{-4}$, Eq. (3.5) may also be written

$$\epsilon=5.3\times 10^{-6}\nu^{-10/3}. \tag{3.6}$$

It will be shown below that the relations (3.5) and (3.6) are not limited to the ideal case of a stationary wind blowing orthogonally offshore, but appear to apply generally for all developing wave spectra, independent of the space-time structure of the wind field and the form of the upwind boundaries. The relations imply that in a growing wind sea the wave spectrum always attains a level for which the nonlinear transfer of momentum from the central region of the spectrum to higher frequencies accounts for about 10–20% of the total momentum transfer across the air-sea interface. The precise value of this ratio is not critical for the constants in (3.5) and (3.6) since c_{hf} enters only to the $\frac{1}{3}$ power. In the following sections we shall develop a simple parametric wave model from which the general validity of (3.5) and (3.6) for growing wind seas can be derived quantitatively.

4. The parametric transport equations

In order to incorporate the nonlinear energy transfer in a numerical wave model, the complex Boltzmann integral expression for S_{nl} needs to be parameterized. Various schemes are conceivable. Apart from methods for approximating the integral itself, the usual approach is to carry out exact integrations of S_{nl} for a subclass of spectra $\hat{F}(f, \theta; a_1, a_2, \ldots, a_n)$ characterized by n free parameters $a_1, a_2, \ldots, a_n$, and to approximate the nonlinear source function for the true spectrum F by the source function from a neighboring member of the class $\hat{F}$. The source functions for $\hat{F}$ may be either stored or approximated by some analytical function of $a_1, a_2, \ldots, a_n$.

The method yields a satisfactory parameterization of S_{nl} only if the class of the spectra $\hat{F}$ yields good approximations for all spectra which arise during the integration of the wave model. If this is the case, however, it is consistent to extend the parameterization technique beyond its immediate application to the nonlinear transfer to all terms in the transport equation. In this manner the true spectrum can be replaced by an appropriate approximation $\hat{F}$ everywhere in the transport equation, and the prediction of the two-dimensional continuum F is reduced to the prediction of a finite number of parameters $a_1, a_2, \ldots, a_n$.

A method for projecting the full transport equation onto a set of prognostic equations for $a_1, a_2, \ldots, a_n$ is described in J. To approximate a given spectrum F by a member of the class $\hat{F}$ some set of algorithms ϕ_i must be introduced which define the best-fit parameters a_i for any given F, i.e., $a_i=\phi_i(F)$. A variation δF in F will then induce a variation δa_i in a_i, which will be related to δF through a linear "projection operator," the functional derivative of ϕ_i, i.e.,

$$\delta a_i=\phi_i'(\delta F). \tag{4.1}$$

Substitution in (4.1) of the specific variation $\delta F=(\partial\hat{F}/\partial a_j)\delta a_j$ for a spectrum from the class $\hat{F}$ yields the relation

$$\phi_i'\left(\frac{\partial\hat{F}}{\partial a_j}\right)=\delta_{ij}. \tag{4.2}$$

The transport equations for the parameters a_i can now be derived by applying the projection operator ϕ_i' to the transport equation (3.2) in the form

$$\frac{\partial\hat{F}}{\partial a_j}\left(\frac{\partial a_j}{\partial t}+v_k\frac{\partial a_j}{\partial x_k}\right)=T,$$

in which the spectrum F has been replaced by its parameterized form $\hat{F}$. Applying the relation (4.2) to the time-derivative term, one obtains

$$\frac{\partial a_i}{\partial t}+D_{ijk}\frac{\partial a_i}{\partial x_k}=S_i, \tag{4.3}$$

where the propagation velocities D_{ijk} and source terms S_i are determined by the advection and source terms in the original transport equation:

$$D_{ijk}=\phi_i'\left(v_k\frac{\partial\hat{F}}{\partial a_j}\right), \tag{4.4}$$

$$S_i=\phi_i'(T). \tag{4.5}$$

A discussion of some of the properties of (4.3) for the case that $a_1, a_2, \ldots, a_n$ correspond to the five parameters of the spectral family (2.1) (with fixed directional distribution) is given in J.

We consider here the simpler case in which both the directional distribution and the spectral shape are prescribed, so that the spectrum contains only two free scale parameters a_1 and a_2. It would be incorrect, however, to derive the prognostic equations for a_1 and a_2 in this case simply by truncating (4.3) at $n=2$. The two-parameter approximation is justified, not because the source functions for the shape parameters $a_3, a_4, \ldots$, vanish, but because the deviations of the shape parameters from their equilibrium values immediately give rise to large restoring terms which rapidly return the shape parameters to their equilibrium values.

This relaxation process will normally be accompanied by a change in the scale parameters a_1, a_2. Thus any terms in the original transport equation (3.2) which tend to change the shape parameters (wind input, dissipation or advection terms) will produce instead indirect changes in the scale parameters. It can be shown that the resulting equations for the evolution of a_1, a_2 are still of the form (4.3) with $n=2$, but the closure procedure yields relations for the propagation velocities and source functions which are more complex than (4.4) and (4.5) and depend on the projection operators ϕ_i' for both scale and shape parameters. An exact evaluation of these relations requires a detailed description of the nonlinear relaxation process responsible for the

shape invariance. Although this is feasible, for the purpose of this paper we shall adopt a simpler closure scheme which reproduces the main features, if not all details, of the relaxation process.

For an invariant spectrum of the form (2.1), the shape parameter $\lambda = \mathcal{E} f_m^4/(\alpha g^2)$ remains constant, so that variations of the scale parameters f_m, α and ϵ are linearly related, i.e.,

$$4\frac{\delta f_m}{f_m} - \frac{\delta\alpha}{\alpha} + \frac{\delta\mathcal{E}}{\mathcal{E}} = 0. \tag{4.6}$$

In general, the various contributions to the source function T, together with the advective term, will produce changes δF of the spectrum in the time increment δt which are projected in the parametrical representation into changes $\delta a_i = \phi_i'(\delta F)$ of the parameters. If the rates of change of the three scale parameters f_m, α and ϵ are determined in this way, the contributions to δf_m, $\delta\alpha$ and $\delta\epsilon$ from different source terms will normally not satisfy (4.6). Nor will the net change satisfy (4.6) unless the shape-restoring nonlinear transfer terms induced by small changes in the shape parameters are specifically included. In other words, the quasi-constancy of the shape parameters comes about dynamically only by specifically including shape-parameter variables in the source functions. It is clear that a rigorous elimination of the shape parameters in a two-parameter wave model must therefore be based on a two-timing treatment, in which the full parametrical equations are integrated over a time t^* which is large compared with the shape response time but small compared with the time scales characterizing the rate of change of the scale parameters. Instead of carrying this out, however, we assume here simply that the changes $\delta f_m'$, $\delta\alpha'$, $\delta\mathcal{E}'$ of the scale parameters, as computed from δF by application of their associated projection operators ϕ_i', are modified after carrying out the intermediate time-scale integration over t^* through additional changes $\delta f_m''$, $\delta\alpha''$, $\delta\mathcal{E}''$, such that the net change $\delta f_m = \delta f_m' + \delta f_m''$, $\delta\alpha = \delta_\alpha' + \delta_\alpha''$, $\delta\mathcal{E} = \delta\mathcal{E}' + \delta\mathcal{E}''$ satisfies (4.6). To make the corrections unique we introduce the minimal condition

$$\left(\frac{\delta f_m''}{f_m}\right)^2 + \left(\frac{\delta\alpha''}{\alpha}\right)^2 + \left(\frac{\delta\mathcal{F}''}{\mathcal{F}}\right)^2 = \min, \tag{4.7}$$

which yields the solutions

$$\left.\begin{aligned} \frac{\delta f_m}{f_m} &= \frac{\delta f_m'}{f_m} - 4\rho \\ \frac{\delta\alpha}{\alpha} &= \frac{\delta\alpha'}{\alpha} + \rho \\ \frac{\delta\mathcal{F}}{\mathcal{F}} &= \frac{\delta\mathcal{F}'}{\mathcal{F}} - \rho \end{aligned}\right\}, \tag{4.8}$$

where

$$\rho = \frac{1}{18}\left(4\frac{\delta f_m'}{f_m} - \frac{\delta\alpha'}{\alpha} + \frac{\delta\mathcal{E}'}{\mathcal{E}}\right).$$

The technique could be carried further by requiring the invariance of additional shape parameters, but in view of the arbitrariness of the side condition (4.7) this hardly appears justified. The shape parameter λ was chosen in order to obtain mutually consistent wave-model representations using either the α-ν or ϵ-ν parameter plane.

Carrying out the computations (4.4), (4.5) and applying (4.8), we obtain for the parameter pair $\nu = f_m U/g$ and α the prognostic equations

$$\underbrace{\frac{1}{\nu}\left(\frac{\partial\nu}{\partial\tau} + P_{\nu\nu}\frac{\partial\nu}{\partial\eta}\right) + P_{\nu\alpha}\frac{1}{\alpha}\frac{\partial\alpha}{\partial\eta}}_{S_{in}} = \underbrace{-N_\nu\alpha^2\nu}_{S_{nl}} + \underbrace{\frac{1}{U}\left(\frac{\partial U}{\partial\tau} + \frac{\partial U}{\partial\eta}\right)}_{\substack{\text{non-uniform} \\ \text{wind field}}}, \tag{4.9}$$

$$\frac{1}{\alpha}\left(\frac{\partial\alpha}{\partial\tau} + P_{\alpha\alpha}\frac{\partial\alpha}{\partial\eta}\right) + P_{\alpha\nu}\frac{1}{\nu}\frac{\partial\nu}{\partial\eta} = I\nu^{7/3} - N_\alpha\alpha^2\nu + \frac{0.2}{U}\left(\frac{\partial U}{\partial\eta}\right), \tag{4.10}$$

where

$$\begin{pmatrix} P_{\nu\nu} & P_{\nu\alpha} \\ P_{\alpha\alpha} & P_{\alpha\nu} \end{pmatrix} = \begin{pmatrix} 1 & -0.07 \\ 0.47 & 0.2 \end{pmatrix}, \quad N_\nu = 0.54, \quad N_\alpha = 5, \quad I = 5.1\times10^{-3},$$

and $\partial/\partial\tau = (U/g)(\partial/\partial t)$, $\partial/\partial\eta = (U/g)\mathbf{V}_m\cdot\nabla$, with $\mathbf{V}_m$ parallel to the wind direction, $|\mathbf{V}_m| = qg/(4\pi f_m)$, $q = 0.85$. The dimensionless gradient $\partial/\partial\eta$ corresponds to the rate of advection of properties with the group velocity $\mathbf{V}_m$ of waves in the spectral peak. The correction factor q arises from averaging over the directional distribution of the spectrum, which was taken here as frequency independent and proportional to the square cosine of the angle θ relative to the local wind direction for $|\theta| \leqslant \pi/2$, and zero in the upwind half-plane $\pi/2 \leqslant |\theta| \leqslant \pi$. Most measurements indicate a frequency-dependent directional distribution with increasing spread at higher frequencies (cf. Mitsuyasu *et al.* 1973, 1975; Tyler *et al.*, 1974). However, the coefficients in

(4.9) and (4.10) are not strongly dependent on the directional distribution, and this effect was ignored. The approximations involved in assuming a fixed directional distribution relative to the mean local wind (thereby eliminating all directional parameters in the prognostic equations) are discussed in Section 7.

It should be noted that the derivatives $\partial/\partial\tau$, $\partial/\partial\eta$ merely represent convenient abbreviations for the non-dimensionalized derivatives with respect to t and the coordinate x_1 parallel to the local wind direction; τ and η are in general non-integrable.

If α is replaced by the energy-scale parameter $\epsilon = \mathcal{E}g^2/U^4$, the equations become

$$\underset{S_{in}}{}\quad \underset{S_{nl}}{}\quad \underset{\text{wind field}}{\text{non-uniform}}$$

$$\frac{1}{\nu}\left(\frac{\partial\nu}{\partial\tau}+0.72\frac{\partial\nu}{\partial\eta}\right)-\frac{0.07}{\epsilon}\frac{\partial\epsilon}{\partial\eta}=-\frac{N_\nu\epsilon^2\nu^9}{\lambda^2}+\frac{1}{U}\left(\frac{\partial U}{\partial\tau}+\frac{\partial U}{\partial\eta}\right), \tag{4.11}$$

$$\frac{1}{\epsilon}\left(\frac{\partial\epsilon}{\partial\tau}+0.75\frac{\partial\epsilon}{\partial\eta}\right)-\frac{0.8}{\nu}\frac{\partial\nu}{\partial\eta}=I\nu^{7/3}-\frac{N_\epsilon\epsilon^2\nu^9}{\lambda^2}-\frac{4}{U}\frac{\partial U}{\partial\tau}-\frac{3.8}{U}\frac{\partial U}{\partial\eta}, \tag{4.12}$$

with

$$N_\epsilon = N_\alpha - 4N_\nu = 2.84.$$

Eqs. (4.11) and (4.12) follow directly from (4.9) and (4.10) using the relation $\lambda = \epsilon\nu^4/\alpha = \text{constant} = 1.6\times10^{-4}$.

The appearance of spatial and time derivatives of the wind field as source terms on the right-hand sides of the equations is due to the use of non-dimensional scale parameters depending on U. These terms do not occur in the original parametric equations (4.3), which refer to variables defined in terms of the wave spectrum alone. However, the transformation from f_m to $\nu = Uf_m/g$, for example, gives rise to additional wind-dependent source terms through relations of the form

$$\frac{1}{f_m}\frac{\partial f_m}{\partial t}=\frac{1}{\nu}\frac{\partial\nu}{\partial t}-\frac{1}{U}\frac{\partial U}{\partial t}, \text{ etc.}$$

The remaining source terms are associated with the direct atmospheric input or the nonlinear transfer, as indicated.

The steps involved in projecting the full transport equation (3.7) onto the transport equations (4.9) and (4.10) [or (4.11) and (4.12)] for two scale parameters may be summarized as follows:

a. Definition of the parameters α, $\mathcal{E}$ and f_m

We have defined the parameter α here as the mean value of the whitened spectrum $E(f)f^5g^{-2}\varphi^{-1}$, including the influence of the shape function

$$\varphi=\exp\left\{-\frac{5}{4}\left(\frac{f_m}{f}\right)^4+\ln\gamma\exp\left[\frac{-(f-f_m)^2}{2\sigma^2f_m^2}\right]\right\},$$

in the range $1.35f_m < f < 2f_m$. Thus α is determined by the level of the spectrum in the immediate falloff region beyond the peak, rather than by the asymptotic, high-frequency range of the spectrum. This is motivated by applications, for which it is generally more important to predict the properties of the energy-containing regions of the spectrum than the short waves. For the same reason $\mathcal{E}$ is defined as the variance of the surface displacement in the range $f<2f_m$. The region beyond $2f_m$ yields only a negligible contribution (5%) to the total variance, and the use of the same cutoff for α and $\mathcal{E}$ has the advantage that in evaluating the source functions one needs consider only processes which affect the spectrum in the frequency range $f<2f_m$. Thus the cutoff in $\mathcal{E}$ is introduced primarily as a conceptual simplification for the derivation of the dynamical transport equations. In practice, it is irrelevant, and in the data presented in Section 10, $\mathcal{E}$ represents the complete variance of the wave field. The peak frequency f_m is defined as the frequency of the maximum of E (not of the whitened spectrum).

b. Calculation of the propagation and nonlinear source terms

Having prescribed the algorithms for determing f_m, α and $\mathcal{E}$ for a given spectrum, the propagation terms D_{ijk} and the nonlinear source terms can be computed according to (4.4) and (4.5). It may be noted that the nonlinear source function for $\mathcal{E}$ in (4.12) is negative rather than zero, as may have been expected from the conservative properties of resonant nonlinear interactions. This is because the positive lobe of the nonlinear source function in the region $f>2f_m$ (cf. Fig. 2) is excluded through our definition of $\mathcal{F}$. The functional forms of the nonlinear source terms in (4.9) and (4.10) follow from the scaling properties of the exact integral expressions for S_{nl}; the coefficients were determined from numerical computations for the mean JCNSWAP spectrum (cf. J and Sell and Hasselmann, 1972).

c. Correction for shape invariance

Next, the propagation and nonlinear source terms were corrected for shape invariance in accordance with

(4.8). The corrected values differed from the original terms by less than 10%, suggesting that the use of (4.8) instead of a more rigorous two-timing analysis is not very critical.

d. Input source functions

To close the energy balance, the input source functions were then computed. The energy balance was taken to be of the form indicated in Fig. 4a, with vanishing dissipation in the main region of the spectrum ($f<2f_m$). (It is shown in Section 8, however, that the neglect of dissipation in the range $f<2f_m$ is unnecessary for the subsequent analysis in which the two-parameter model is further reduced to a single parameter.) In accordance with most theories of wave generation based on linear feedback mechanisms, S_{in} was assumed proportional to the wave spectrum, i.e., $S_{in}=\beta f E(f)$, where β is a function of the parameter Uf/g only. This yields an input source function for α of the form $\alpha\psi(\nu)$, where the function $\psi(\nu)$ depends on the functional form of β. The influence of the atmospheric input on the rate of shift of the peak frequency ν was negligible compared with the nonlinear terms in (4.9) and (4.10). The rate of shift of the peak is controlled by the difference in energy gained on both sides of the peak. If β is a reasonably smoothly varying function, the input source function, being proportional to the spectrum itself, will be approximately symmetrical relative to the peak. On the other hand, S_{nl} has an extremely pronounced plus-minus asymmetry across the peak. For typical β functions the rate of migration of the peak induced by S_{nl} is two orders of magnitude larger than the contribution from S_{in}. Since the dissipation source terms were assumed zero in the range $f<2f_m$, this leaves $\psi(\nu)$ as the only unknown function in the parametric equations, and this can then be determined by comparison with fetch-limited growth data. For consistency, the empirical power laws (2.2) and (2.3) were slightly modified to the power laws

$$\nu=2.84\,\xi^{-0.3}, \tag{4.13}$$

$$\alpha=0.0662\,\xi^{-0.2}, \tag{4.14}$$

to yield a fetch-independent value of 1.58×10^{-4} for the shape parameter λ, as required for shape invariance. [On elimination of the fetch, Eqs. (4.13) and (4.14) yield the same relations (3.5) and (3.6) between the scale parameters as before.]

5. Special solutions

The integration of Eqs. (4.9), (4.10) or (4.11), (4.12) for an arbitrary wind field $U(x,t)$ under appropriate boundary and intitial conditions can only be carried out numerically However, it is instructuve to consider two special classes of wind fields for which solutions can be given analytically. If the wind field depends on only fetch x or duration t according to power laws

$$\text{(a)}\quad U=U_0(gx/U_0^2)^p, \tag{5.1}$$

$$\text{(b)}\quad U=U_0(gt/U_0)^q, \tag{5.2}$$

with $U_0=$ constant, the parametrical transport equations permit simple power-law solutions of the form

$$\text{(a)}\quad \nu=A(gx/U_0^2)^m,\quad m=\tfrac{3}{10}(2p-1), \tag{5.3}$$

$$\text{(b)}\quad \nu=A(gt/U_0)^n,\quad n=3/7(q-1), \tag{5.4}$$

where in both cases

$$\alpha=B\nu^3, \tag{5.5}$$

$$\epsilon=C\nu^{-10/3}, \tag{5.6}$$

with constant A, B and C.

Eq. (5.6) and the coefficient $C=B\lambda$ follow from (5.5) and shape invariance, $\lambda=\epsilon\nu^4/\alpha=$ constant. The remaining coefficients are given by

$$\text{(a)}\quad \begin{cases} A=2.84(1+1.63p)^{3/10} & (5.7)\\ B=0.033\left(\dfrac{1+1.50p}{1+1.63p}\right)^{\frac{1}{2}} & (5.8)\end{cases}$$

or

$$\text{(b)}\quad \begin{cases} A=16.8(1+1.51q)^{3/7} & (5.9)\\ B=0.031\left(\dfrac{1+1.33q}{1+1.51q}\right)^{\frac{1}{2}}. & (5.10)\end{cases}$$

The solutions satisfy the initial condition of vanishing energy $\mathcal{E}=\epsilon U^4/g^2=0$ at $x=0$ [case (a)] or $t=0$ [case (b)] for $p>-\frac{1}{2}$ or $q>-5/9$, respectively. If the exponents become more negative than these values the singularity of the wind field at $x=0$ or $t=0$ becomes so strong that the wave-field solutions also become singular initially.

For $p=0$, case (a) reduces to the uniform-wind, fetch-limited case, and Eqs. (5.3) – (5.8) become identical with Eqs. (3.5), (3.6), (4.13), (4.14), and (2.4).

It is interesting to note that the power-law relations between α, ϵ and ν are independent of the exponents p or q and are identical for the fetch-limited and duration-limited cases. Moreover it is apparent from Fig. 5 that the coefficient B (and therefore also C) varies by only a few percent within a wide range of exponents p, q and is almost the same for both cases (a) and (b). Thus for practical purposes the wave field can be characterized for both classes of wind fields by the fetch or duration dependence of a single parameter, ν, say (Fig. 6). It is shown in the following that the reduction of the two-parameter description of the wave field to a single parameter applies generally and is not limited to the particular solutions considered here.

6. The single-parameter approximation

The reason for the weak wind-field dependence of the relations (5.5) and (5.6) becomes apparent on inspection

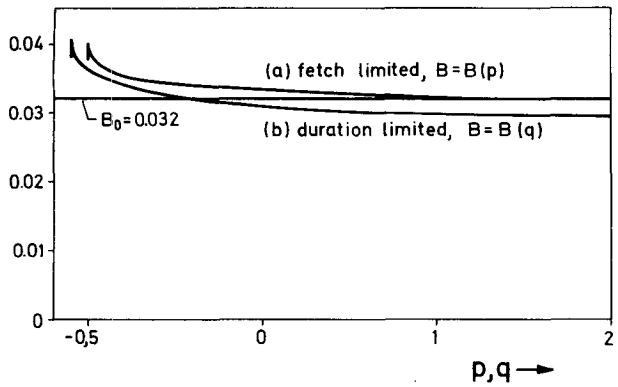

FIG. 5. The coefficient B in the relation $\alpha = B\nu^{\frac{1}{2}}$ for the case of (a) a fetch-limited wave field with wind field $U = U_0(gx/U_0^2)^p$ and (b) a duration-limited wave field with wind field $U = U_0(gt/U_0)^q$. The value $B_0 = 0.032$ corresponds to the quasi-equilibrium relation (6.1).

of (4.9) and (4.10). The nonlinear interaction term for ν in (4.9) is an order of magnitude smaller than the corresponding nonlinear source term in (4.10) for α. On the other hand, the propagation terms on the left-hand sides of the equations are governed by the response scales of ν and α with respect to τ or η, and for power-law solutions are of the same order for both ν and α. The source terms due to the wind-field variation are also of this order. Thus the nonlinear interaction term in the prognostic equation for α is large compared with both the propagation and wind-variation terms, and can be balanced only by the remaining wind-generation term. To first order, Eq. (4.10) therefore yields

$$\alpha = B_0\nu^{\frac{1}{2}}, \quad B_0 = (I/N_\alpha)^{\frac{1}{2}} = 0.032. \tag{6.1}$$

The equivalent expression in terms of the energy is given by

$$\epsilon = C_0\nu^{-10/3}, \quad C_0 = B_0\lambda = 5.1\times 10^{-6}. \tag{6.2}$$

Eqs. (6.1) and (6.2) lie within a few percent of the exact solutions (5.5)–(5.10) for power-law wind fields [and the empirical relations (3.5) and (3.6)].

Physically, the quasi-equilibrium relations (6.1) and (6.2) express the fact that the dominant balance determining the level of the spectrum in the central region of the spectrum is between the atmospheric input and the nonlinear transfer of energy away from the central region of the spectrum to high frequencies (beyond $2f_m$) and to frequencies lower than the peak frequency. The adjustment process is stable, since the energy input is linear with respect to the wave spectrum, whereas the nonlinear transfer is cubic. Thus an increase in the input through an increase in wind speed increases the spectrum to a new level at which the more rapidly increasing nonlinear transfer is again able to balance the input. Estimates given in the next section indicate that this energy-level adjustment occurs almost as rapidly as the nonlinear shape stabilization. Since the distributions of the nonlinear and input source functions differ in detail, the balance applies only in an average sense, not as a detailed equilibrium for each frequency. In particular, the narrow plus-minus signature of the nonlinear source function in the vicinty of the peak cannot be matched by the more smoothly varying input and results in a net transfer of energy from the rear to the forward face of the peak. However, the migration of the peak to low frequencies is a slow process compared with the adjustment of the spectrum to its stable quasi-equilibrium shape and level. Thus to first order the latter can be treated as local equilibrium processes, and on the time and space scale of typical wind fields the prediction problem reduces to the integration of the peak-frequency equation.

The quasi-equilibrium relations (6.1) and (6.2) suggest a simple perturbation method for constructing approximations to the general solutions of (4.9) and (4.10) [or (4.11) and (4.12)] by expanding α and ν in series:

$$\alpha = \alpha_0 + \Delta\alpha_1 + \Delta^2\alpha_2 + \ldots,$$
$$\nu = \nu_0 + \Delta\nu_1 + \Delta^2\nu_2 + \ldots,$$

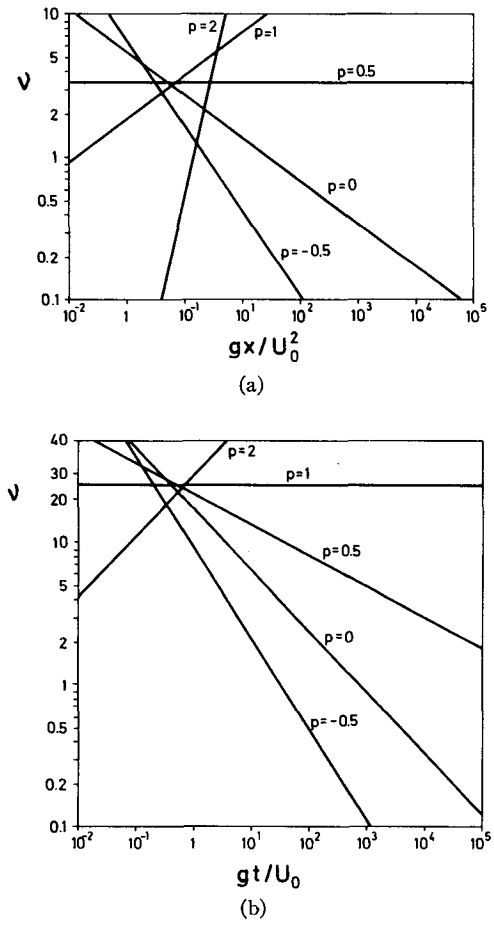

FIG. 6. Development of the non-dimensional peak frequency $\nu = Uf_m/g$ as a function of (a) fetch and (b) duration for various power-law wind fields $U = U_0(gx/U_0^2)^p$ and $U = U_0(gt/U_0)^q$, respectively.

where $\Delta \ll 1$, $\alpha_n = O(\alpha_0)$, $\nu_n = O(\nu_0)$, and α_0, ν_0 satisfy (6.1). The coefficient Δ represents the ratio of a typical term in the transport equations (4.9) and (4.10) (for example, the nonlinear interaction term $N_\nu \alpha^2 \nu$ in the ν equation) to either of the two dominant terms in the α equation (for example, the nonlinear interaction term $N_\alpha \alpha^2 \nu$). In the following we set $\Delta = N_\nu / N_\alpha$. Substituting the perturbation series in Eqs. (4.9) and (4.10) and ordering in powers of Δ, one obtains a sequence of uncoupled equations which can be solved individually at each expansion step.

Expressing α_0 in Eq. (4.9) in terms of ν_0 using (6.1), the zero-order equation for ν_0 is obtained as

$$\frac{1}{\nu_0}\left(\frac{\partial \nu_0}{\partial \tau} + P_0 \frac{\partial \nu_0}{\partial \eta}\right) = -N_0 \nu_0^{7/3} + \frac{1}{U}\left(\frac{\partial U}{\partial \tau} + \frac{\partial U}{\partial \eta}\right), \quad (6.3)$$

where

$$P_0 = P_{\nu\nu} + \tfrac{2}{3} P_{\nu\alpha} = 0.95,$$

$$N_0 = N_\nu B_0^2 = 5.5 \times 10^{-4}.$$

The subsequent higher order equations are linear. For α_1, one obtains

$$\frac{1}{\alpha_0}\left(\frac{\partial \alpha_1}{\partial \tau} + P_{\alpha\alpha} \frac{\partial \alpha_1}{\partial \eta}\right) + \frac{\alpha_1}{\tau_e \alpha_0} = -L(\nu_0) + \frac{0.2}{U} \frac{\partial U}{\partial \eta}, \quad (6.4)$$

where

$$\left.\begin{aligned} \tau_e &= (2 N_\alpha \alpha_0^2 \nu_0)^{-1} \\ L(\nu_0) &= -\frac{1}{\alpha_0}\left(\frac{\partial \alpha_0}{\partial \tau} + P_{\alpha\alpha} \frac{\partial \alpha_0}{\partial \eta}\right) + P_{\alpha\nu} \frac{\partial \nu_0}{\partial \eta} \\ &= -\frac{1}{\nu_0}\left(0.67 \frac{\partial \nu_0}{\partial \tau} + 0.51 \frac{\partial \nu_0}{\partial \eta}\right) \end{aligned}\right\}. \quad (6.5)$$

The solution of (6.4) can be substituted in the next order equation for ν to obtain a correction term ν_1 for ν, from which a second-order correction α_2 can be determined, and so forth.

For practical purposes the zero-order prognostic equation (6.3) for ν, together with the equilibrium equation (6.1) for α, should yield an adequate approximation. An advantage in terminating the expansion after the lowest order is that it can be shown that the zero-order equations are independent of the hypotheses made in closing the spectral energy balance (cf. Section 8), whereas the higher order corrections depend on the details of the input and dissipation source functions balancing the nonlinear energy transfer in the central region of the spectrum (cf. Figs. 4a and 4b).

7. Response scales

The equation for the first-order perturbation α_1 is of interest, as it describes the rate at which α returns to its near-equilibrium value α_0, if the wave state is slightly perturbed from its quasi-equilibrium level [Eq. (6.1)]. Thus it defines the conditions for the validity of the local equilibrium relations (6.1) and (6.2). Changes in the peak frequency and wind field produce forcing terms, represented by the right-hand side of (6.4), which induce changes in α relative to its quasi-equilibrium value α_0. The left-hand side of (6.4) then defines a non-dimensional relaxation time (or equivalent space scale) τ_e for the response of α to these terms. Ignoring for the present the influence of the changing wind field, the ratio of the relaxation time τ_e to the characteristic time scale $\tau_\nu = (N_0 \nu_0^{7/3})^{-1}$ for the migration of the peak frequency [as determined by the zero-order equation (6.3)] is given by $\tau_e / \tau_\nu = N_\nu / 2N_\alpha = \Delta/2$. Thus the response of the perturbation α to the frequency forcing term on the right-hand side of (6.4) is an order of magnitude faster than the rate of change of the zero order fields ν_0 and α_0. To lowest order α_1 is therefore given by the quasi-stationary equilibrium solution

$$\alpha_1 = \tau_e \alpha_0 \left[-L(\nu_0) + \frac{0.2}{U} \frac{\partial U}{\partial \eta}\right], \quad (7.1)$$

for which the assumed inequality $\alpha_1 \ll \alpha_0$ can be verified directly. If the characteristic space or time scales L, T of the forcing term associated with the wind field are smaller than the corresponding peak-frequency scales, the condition $\tau_e / \tau_\nu \ll 1$ for the validity of (7.1) must be replaced by the appropriate space or time response inequality (whichever is the more stringent)

$$\tau_e \ll \frac{4\pi\nu}{q P_{\alpha\alpha}} \frac{gL}{U^2} \approx 30 \frac{\nu g}{U^2} L \quad (7.2)$$

or

$$\tau_e \ll \frac{g}{U} T, \quad (7.3)$$

where $q = 0.85$ is the direction correction factor defined after Eq. (4.10). Substitution of (6.5) and (6.1) yields

$$L \gg \frac{3U^2}{g} \nu^{-10/3}, \quad (7.4)$$

$$T \gg \frac{100U}{g} \nu^{-7/3}. \quad (7.5)$$

For a growing sea, ν lies typically in the range $0.15 < \nu < 1$. Taking the least favorable (nearly fully developed) value $\nu = 0.15$, Eqs. (7.4) and (7.5) yield $L \gg 1.6 \times 10^3 U^2/g$ and $T \gg 8 \times 10^3 U/g$. For $U = 10$ m s^{-1}, for example, the α response can therefore be regarded as quasi-local if $L \gg 16$ km and $T \gg 2.3$ h. The corresponding conditions for a less fully developed sea with $\nu = 0.3$ become $L \gg 1.7$ km and $T \gg 0.5$ h. The values suggest that except for very rapid wind changes and well-developed wind seas, the energy level of the spectrum can be determined to good approximation from

the peak frequency using the local equilibrium relation (6.1).

The rate of adjustment to the equilibrium level may be compared with the rate at which the spectrum attains its equilibrium shape. The expression for the rates of change of the shape parameters $s_j=\gamma$, σ_a or σ_b due to the nonlinear energy transfer can be shown to scale in the same way as the corresponding nonlinear source terms for the parameters ν, α and ϵ: $ds_j/dt=N_j\alpha^2\nu$, where the coefficients N_j depend on the shape parameter only. By assumption, all N_j vanish when the shape parameters take their equilibrium values s_j^e. The rate of return to the equilibrium shape for a deviation from the equilibrium depends on the initial deviation. For small displacements from the equilibrium, the coefficients N_j can presumably be expanded in a Taylor series: $N_j=M_{jk}(s_k-s_k^e)$, where $M_{jk}=\partial N_j/\partial s_k$ at the equilibrium point. Thus the shape response of the spectrum near equilibrium is governed by the linear set of equations

$$\frac{ds_j}{dt}=M_{jk}(s_k-s_k^e).$$

This will generally have three eigensolutions, whose eigenvalues λ_j define three relaxation times $\tau_i=\lambda_j^{-1}$.

A systematic analysis of the structure of M_{jk} has not been carried out, but numerical experiments with various initial deviations from the equilibrium shape (which will normally correspond to a superposition of eigensolutions) yielded relaxation times typically of order $\frac{1}{5}$ of the relaxation time τ_e for the adjustment to an equilibrium energy level. Thus the conditions for a local shape equilibrium appear to be still better satisfied than for a local quasi-equilibrium of the spectral energy level (as implicit in our derivation of the one-parameter model via a two-parameter model).

In conclusion, we note that the concept of a local quasi-equilibrium spectrum justifies *a posteriori* the treatment of the directional parameters as given rather than independent prognostic variables. Since the adjustment of the spectrum to its equilibrium level is governed by the local balance between atmospheric input and nonlinear transfer, the directional distribution in the central equilibrium region of the spectrum will adopt a universal form (depending on the directional properties of these balancing processes) in which the mean propagation direction of the waves must be determined by the only external directional parameter, the mean wind direction. Furthermore, the migration of the peak of the spectrum is determined by the nonlinear transfer of energy from the central region of the spectrum across the forward face of the spectrum. Thus the central region of the spectrum determines the reference direction for the newly generated waves at lower frequencies, and hence these will also have directional properties defined relative to the local wind direction. Within the approximation of a quasi-equilibrium spectrum, the directional distribution of the entire wave spectrum can therefore be regarded as a given function (depending in general on the nondimensional frequency f/f_m and peak frequency ν) which is oriented with respect to the local mean wind direction.

8. Independence of the single-parameter model on the energy balance closure

It was pointed out in Section 3 that measurements of the spectral energy balance in fetch-limited wave-growth studies yield only the sum $S_s=S_{in}+S_{ds}$ of the input and dissipation terms of the net source function $S=S_{in}+S_{nl}+S_{ds}$, and that direct measurements of the atmospheric input are still too uncertain to establish the relative contribution of the input and dissipation to S_s. Fortunately, the zero-order single-parameter prediction equation turns out to be independent of the structural form of S_s.

The analysis of the previous sections was based on a minimal-input energy balance with vanishing S_{ds} and a linear dependence of S_{in} on F in the main region of the spectrum ($f\leqslant 2f_m$). Consider now the modifications incurred if the function S_s is arbitrary. In the projection of the complete transport equation (3.2) onto the parameter plane ν, α, the ν equation remains unchanged, since the argument in Section 4 that the nonlinear source function dominates the rate of migration of the peak is independent of the detailed structural form of S_{in} and S_{ds}. The α equation now becomes

$$\frac{1}{\alpha}\left(\frac{\partial\alpha}{\partial\tau}+P_{\alpha\alpha}\frac{\partial\alpha}{\partial\eta}\right)+P_{\alpha\nu}\frac{1}{\nu}\frac{\partial\nu}{\partial\eta}=r-N_\alpha\alpha^2\nu+\frac{0.2}{U}\left(\frac{\partial U}{\partial\tau}+\frac{\partial U}{\partial\eta}\right), \quad (8.1)$$

where the previous input source function in (4.10) has been replaced by an arbitrary function $r(\alpha,\nu)$ determined by the sum source function S_s. (If the dynamics of surface waves depends only on the external parameters g and U, it follows by dimensional analysis that for a constant-shape spectrum the dependence of r on the wind speed can enter only in combination with the peak frequency f_m in the form of the non-dimensional parameter $\nu=f_mU/g$. A possible dependence of wave growth on additional external parameters, or on wind speed independent of f_m, was investigated in JONSWAP, but not detected.)

As in Eq. (4.10), the nonlinear term $N_\alpha\alpha^2\nu$ in Eq. (8.1) is an order of magnitude larger than the observed rate of change of α or the source term arising from the variable wind field. It follows that to first order this term must be balanced by the combined input and dissipation, $r(\alpha,\nu)=N_\alpha\alpha^2\nu$. The relation can be solved for α to yield $\alpha=\alpha(\nu)$. The functional dependence of α on ν can then be determined empirically from fetch-limited wave-growth data, which yields as before the power-law

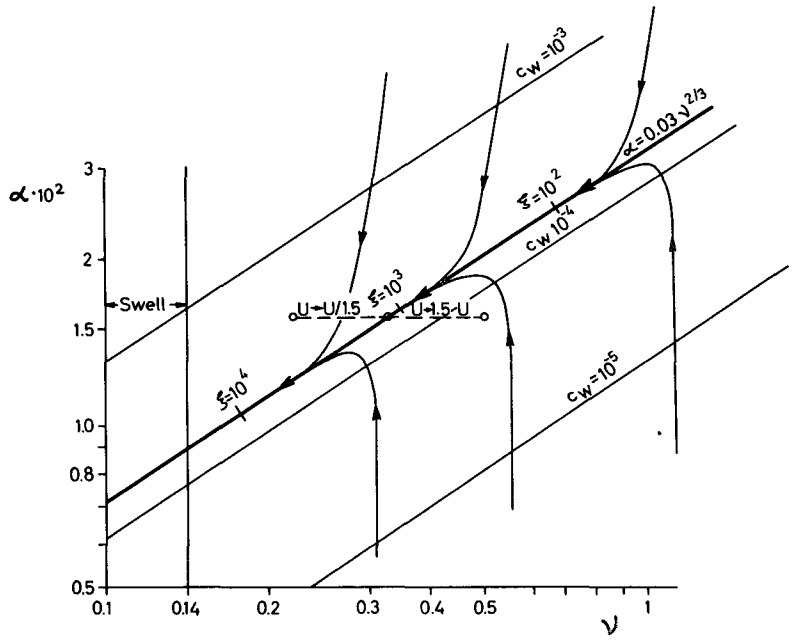

FIG. 7. Evolution of the wave field in the α-ν phase plane. The thick line represents the quasi-equilibrium relation (6.3). Tick marks on the line denote fetch values for the fetch-limited solutions (4.11). Converging thin lines represent solutions of the two-parameter model for non-equilibrium initial states. Also shown are the initial displacements induced in the wave state by a step function change in the wind field by a factor of 1.5 or 1/1.5. The parallel constant c_w lines apply for the case of a minimal-input energy balance.

relation (3.5) [or (6.1)]. This forms the basis of the one-parameter model and the subsequent analysis follows unchanged. Thus the existence of a quasi-equilibrium between the nonlinear transfer and the combined influence of atmospheric input and dissipation always implies a universal relationship between α and ν, independent of the detailed structure of the input and dissipation source functions.

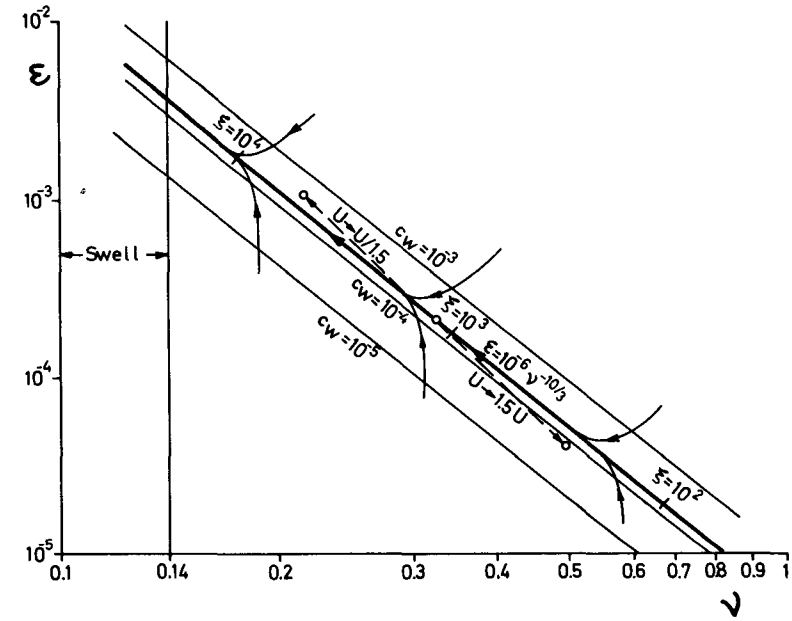

FIG. 8. Evolution of the wave field in the ϵ-ν phase plane. The notation is the same as in Fig. 7.

A, JONSWAP ORTHOGONAL FETCH

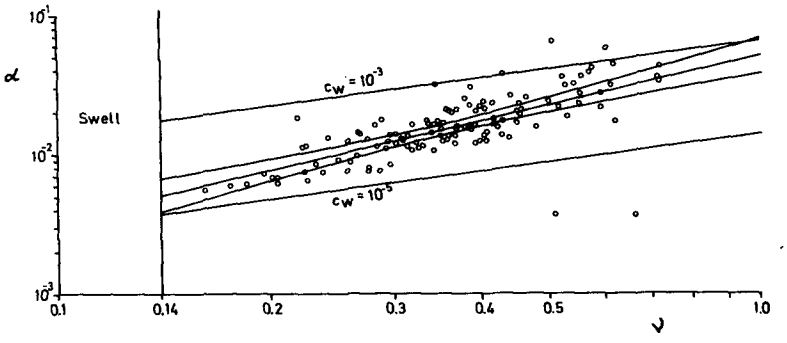

B, W. ATLANTIC FETCH LIMITED

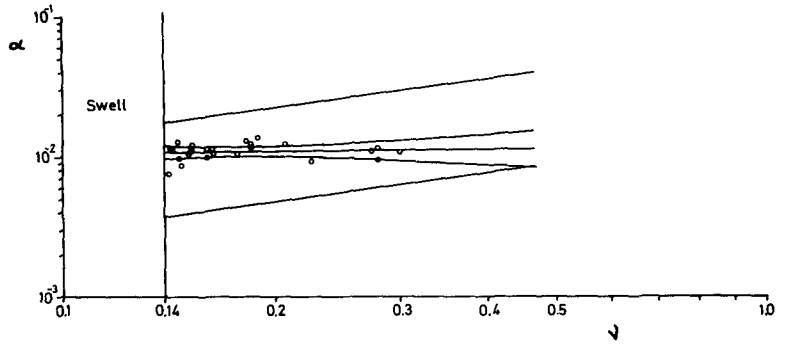

C, JONSWAP SLANTING FETCH

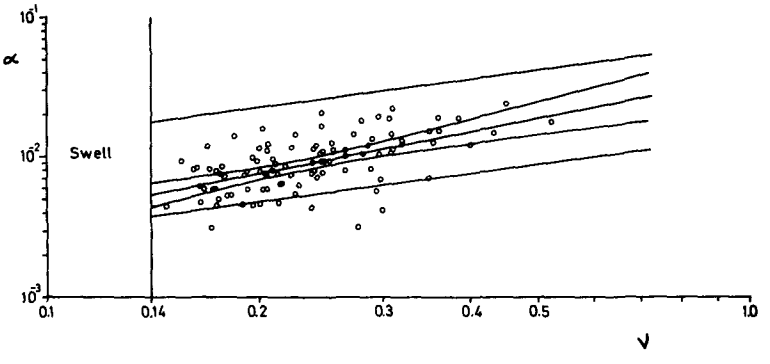

D, ATLANTIC WEATHER SHIPS

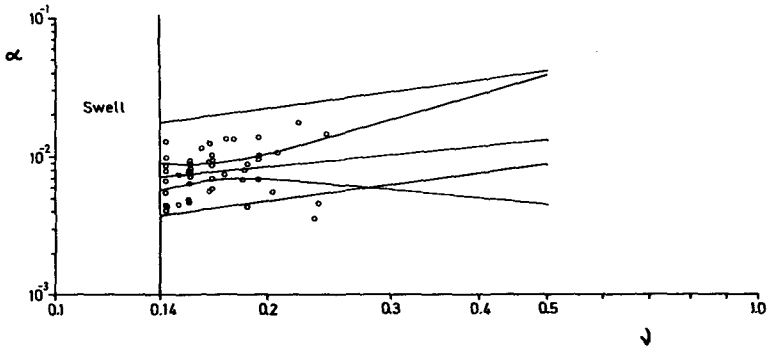

E, WEATHER ADVISER

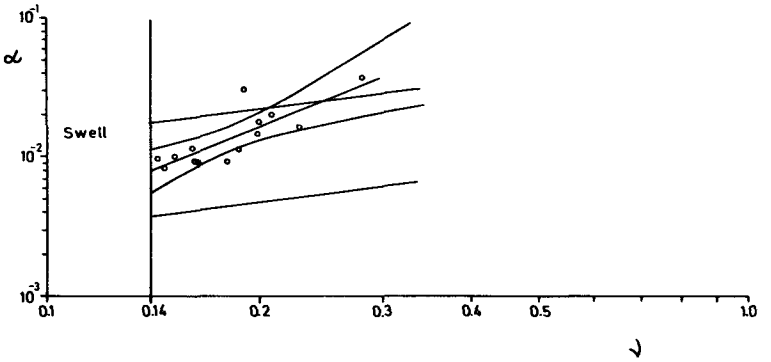

F, ARGUS ISLAND

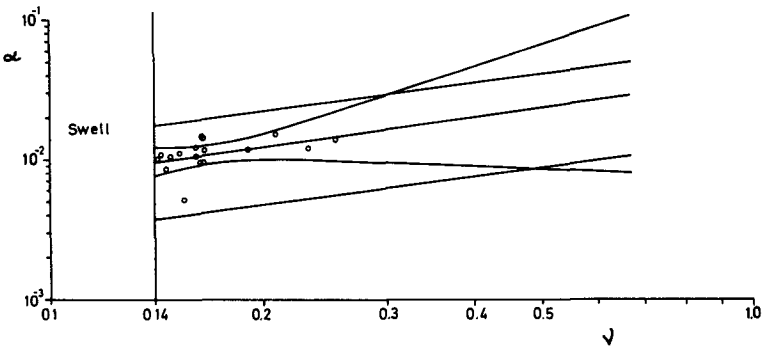

G, HIGH WIND CASES

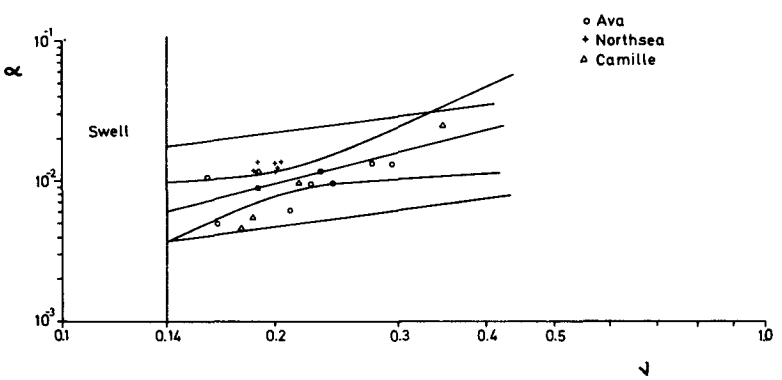

H, LOW WAVE HEIGHTS

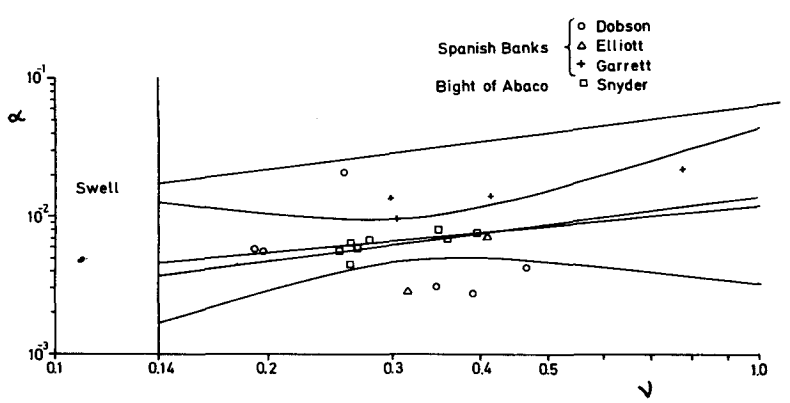

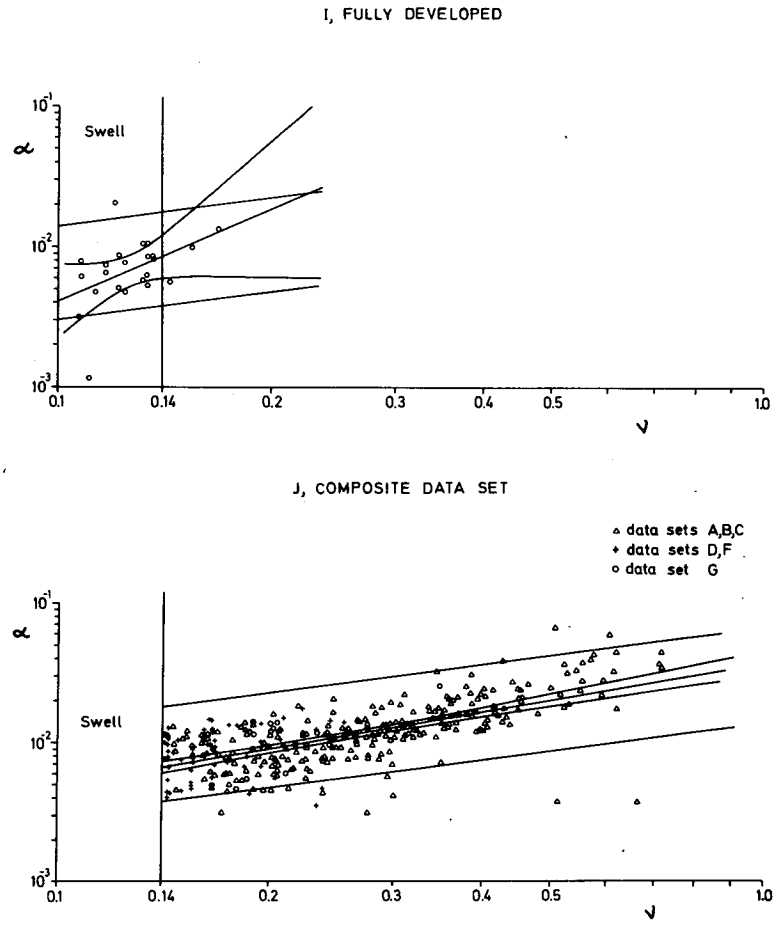

FIG. 9. α-ν plots for the data sets A through J listed in Table 1. Straight lines flanked by hyperbolas represent regression lines and their standard deviation envelopes. Parallel lines correspond to constant wave-induced drag coefficients c_w for a minimal-input energy balance.

The calculation of the relaxation time τ_e for the establishment of the quasi-equilibrium in Section 7 depends numerically on the form of $r(\alpha,\nu)$, but the order of magnitude is insensitive to the structure of r. Essential for the existence of a stable equilibrium is that an increase $\delta\alpha$ in α produces an increase $\delta(N_\alpha\alpha^2\nu)=2N_\alpha\alpha\nu\delta\alpha$ in the nonlinear source term in (8.1), which is larger than the increase $\delta\tau=\partial r/\partial_\alpha\delta\alpha$ induced in r. A small deviation from equilibrium then results in a positive restoring force. For small perturbations, the return to equilibrium is a decaying exponential, and the associated relaxation (e-folding) time is given by $\tau_e=[2N_\alpha\alpha^2\nu-\alpha(\partial r/\partial\alpha)]^{-1}$. This is of the same order as the expression considered in Sections 6 and 7 for the special case $\partial r/\partial\alpha=0$ provided that the two terms in the brackets do not approximately balance, i.e., provided the equilibrium is not marginal. (In fact, if r includes nonlinear dissipative terms, it may be expected that r increases more slowly with α than in the case that r consists of the atmospheric input alone. The equilibrium is then stabler and the relaxation time τ_e smaller than estimated in Section 7.)

9. The phase plane

It is helpful to visualize the parametric wave growth relations in the α-ν and ϵ-ν phase planes (Figs. 7 and 8). The thick lines represent the quasi-equilibrium relations (6.1) and (6.2), while the thin curves converging to the quasi-equilibrium lines describe the approach to equilibrium for wave states which lie off the equilibrium curve initially. The curves represent solutions of the two-parameter model (Section 4) for the case of a constant wind field. In order to describe the convergence toward equilibrium through characteristic curves in the phase plane, the general two-dimensional τ, η dependence of the solutions has to be reduced to a single parameter τ or η by assuming a duration-limited or fetch-limited geometry. The characteristic curves in Figs. 7 and 8 correspond to the duration-limited case in which a uniform deviation from equilibrium is assumed at some initial time. Qualitatively similar curves are found also for the fetch-limited case, where a time-independent non-equilibrium initial wave state is prescribed along some upwind boundary orthogonal to the wind direc-

tion. After adjustment to the asymptotic equilibrium curve, the wave field develops along the equilibrium line in the direction of decreasing ν with increasing duration or fetch, as indicated in the figures. [In fact, the equilibrium curves for the duration-limited and fetch-limited cases differ slightly, but the difference is only a few percent; cf. Eqs. (5.5)–(5.10) for $p=q=0$. In the one-parameter model, the distinction between the two equilibrium curves is, of course, lost.]

To interpret the effect of a variable wind field, consider now the simplest case in which a sudden step-function change in the wind field occurs with respect to fetch or duration (depending on the particular initial-value problem considered) in an otherwise uniform stationary wind field. Since the response of the wave field to the change in wind requires a finite time, the immediate effect of the step-function change is to shift the wave state from a point on the equilibrium line (assuming equilibrium had been established) to an off-equilibrium position simply through the wind speed dependence of the nondimensional variables ν and ϵ (cf. Figs. 7 and 8). Subsequently, the point will then move back to a new position on the equilibrium curve along a converging characteristic trajectory. If the rate of convergence is sufficiently rapid, a continuous sequence of small changes in the wind speed will produce only a small net displacement from the equilibrium line, but because the direction of the displacing and restoring forces differ, the wave state will wander along the equilibrium line. The net movement along the equilibrium line is given by the sum of the wind-variability and nonlinear transfer terms in (6.3). An increasing wind tends to offset the decrease of ν due to the nonlinear transfer and can even lead to an increase of ν with fetch or duration, as demonstrated by the power-law solutions (5.3) for $p>\frac{1}{2}$ and (5.4) for $q>1$ (cf. Figs. 6a and 6b). Conversely, a decreasing wind speed produces a still more rapidly decreasing ν. For example, the rate of decay of the wind speed rather than the nonlinear transfer is normally the dominant term determining the speed of transition from the wind-sea region ($\nu>0.14$) into the swell region ($\nu<0.14$) of the phase plane near $\nu=0.14$.

For the case of a minimum-input energy balance (Fig. 4a), the equilibrium lines in Figs. 7 and 8 correspond to a wave-induced drag coefficient $c_w\approx 0.2\times 10^{-3}$ (about 20% of the total drag coefficient $c_{10}\approx 10^{-3}$). The stability of the equilibrium line can be inferred from the set of displaced equilibrium lines resulting from a changed energy input corresponding to the (minimal) wave-induced drag coefficients $c_w=10^{-4}$, 10^{-3} and 10^{-2}. To alter the equilibrium level significantly, rather large changes in the input from the atmosphere are required. An alternative energy balance with appreciable dissipation in the central region of the spectrum would affect the values of the wave-induced drag coefficient inferred from the equilibrium line, but, as pointed out in the previous section, the stability of the equilibrium line itself remains of the same magnitude (or, if anything, is increased).

Figs. 7 and 8 should be kept in mind in interpreting the data presented in the next section. Most points lie between the parallels $c_w=10^{-3}$ and $c_w=10^{-5}$, which is not surprising when one considers that this band spans a 100:1 change in the equivalent atmospheric input to the wave spectrum.

10. Comparison of the quasi-equilibrium relations with field data

Figs. 9 and 10 show the data distributions in the α-ν and ϵ-ν phase planes for the data groups listed in Table 1. Also shown are the log-log regression lines and the associated standard-deviation hyperbolas (cf. Section 2). The regression line parameters are included in Table 1 (the notation is the same as used for the shape parameters). To avoid congesting the figures, the theoretical equilibrium lines (6.1), (6.2) are not shown, but they lie approximately midway between the parallel lines corresponding to the (minimal) wave-induced drag coefficients $c_w=10^{-3}$ and $c_w=10^{-5}$ (cf. Figs. 7 and 8).

Because of anomalous γ values the *Weather Adviser* data set E has not been included in the composite data set J. Similarly, the large scatter of the α values for the Spanish Banks data and the small α values for the Bight of Abaco spectra let this data set appear rather suspect, and it has therefore also been excluded from J. The wave model is not applicable to the fully developed spectra I, which are shown only for comparison and are similarly not incorporated in J.

Plots of the regression line parameters r, $\log\alpha_0$ and r, $\log\epsilon_0$ for all data sets except E, H and I are shown in Figs. 11 and 12. Rectangles with half-side length equal to the standard deviations of r, $\log\alpha_0$ or r, $\log\epsilon_0$ indicate the statistical uncertainty of the regression line estimates. It should be noted that the indeterminacy of the regression line parameters reflects not only the scatter of individual data points, but also the size of the ensemble for which the regression line is defined. The standard deviations are approximately proportional to the inverse square root of the number of data points. Thus large data sets tend to have better defined regression line parameters. (Since the parameter deviations are generally correlated, it would have been more correct to draw rectangles oriented with respect to rotated axes corresponding to statistically orthogonal variables. However, this was not done as the rotation angles were typically only a few degrees.) The scatter of the individual points of a data set relative to the regression line is indicated by the vertical error bars. The half-lengths of the error lines represent the standard deviation of the vertical displacements of the points from the regression line. It is possible to represent this scatter in the regression-line parameter plane, since the

A, JONSWAP ORTHOGONAL FETCH

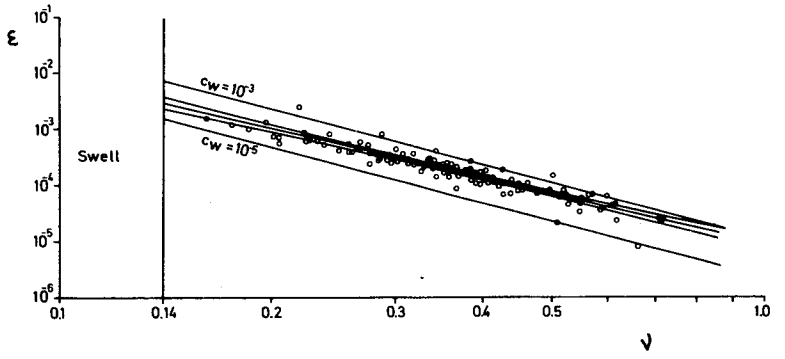

B, W. ATLANTIC FETCH LIMITED

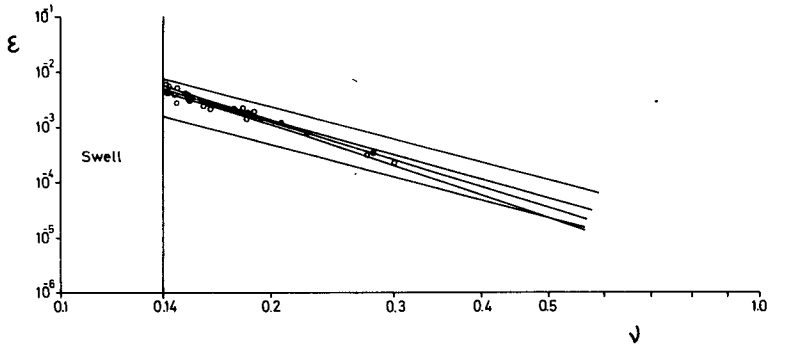

C, JONSWAP SLANTING FETCH

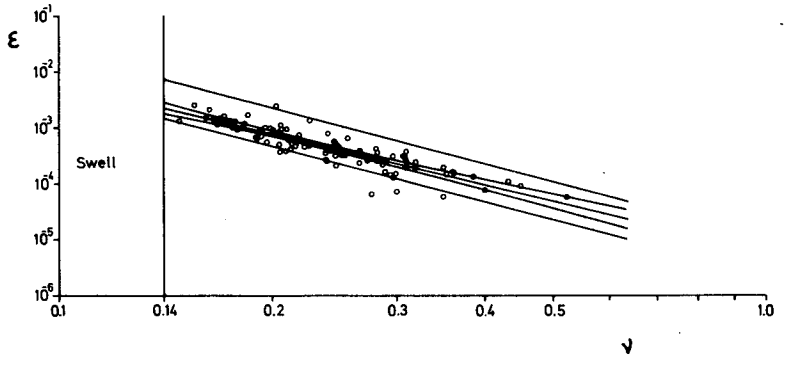

D, ATLANTIC WEATHER SHIPS

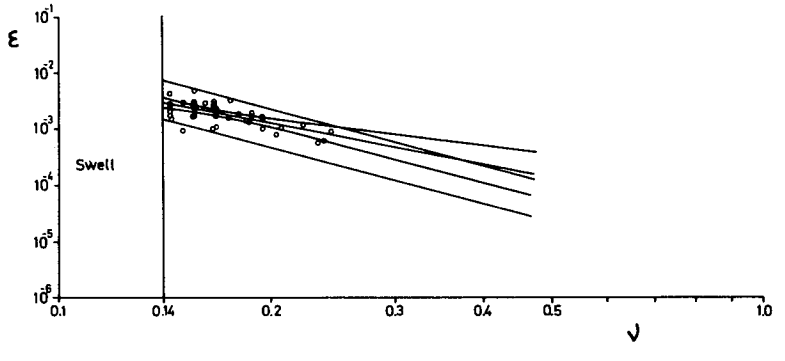

E, WEATHER ADVISER

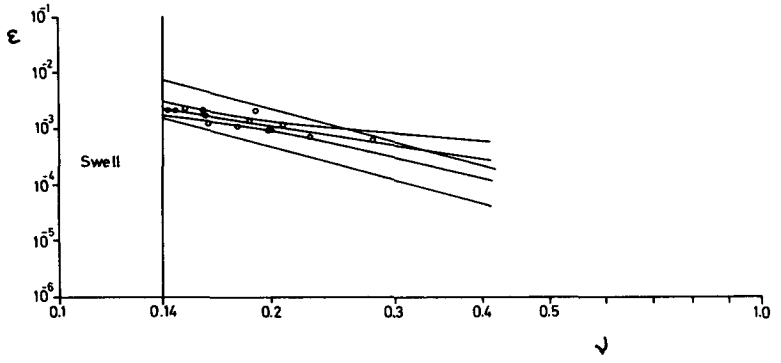

F, ARGUS ISLAND

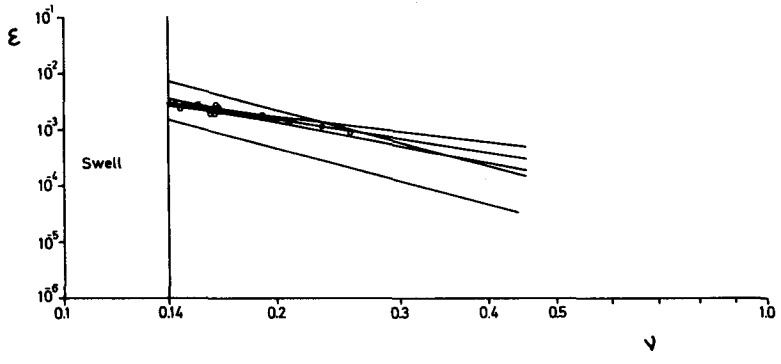

G, HIGH WIND CASES

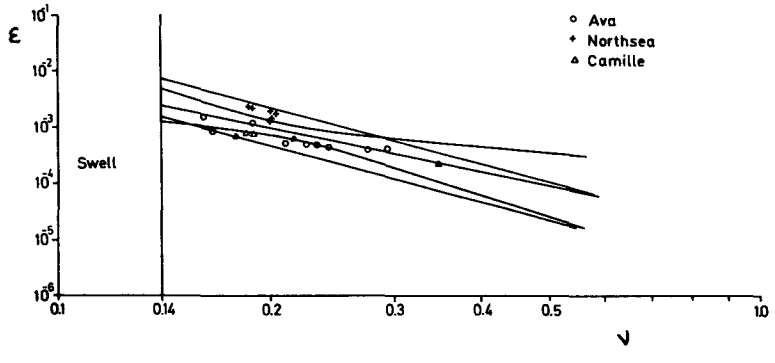

H, LOW WAVE HEIGHTS

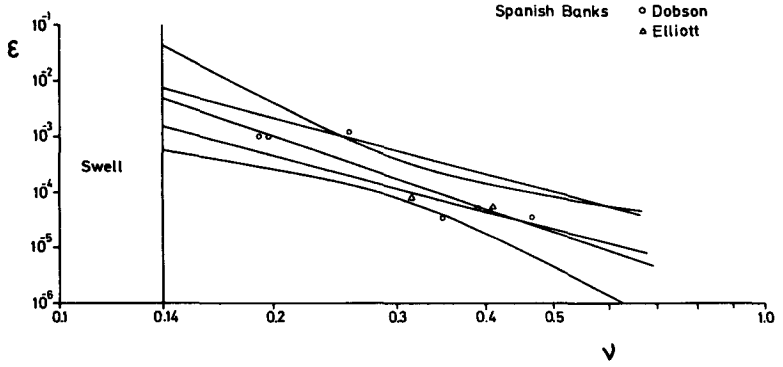

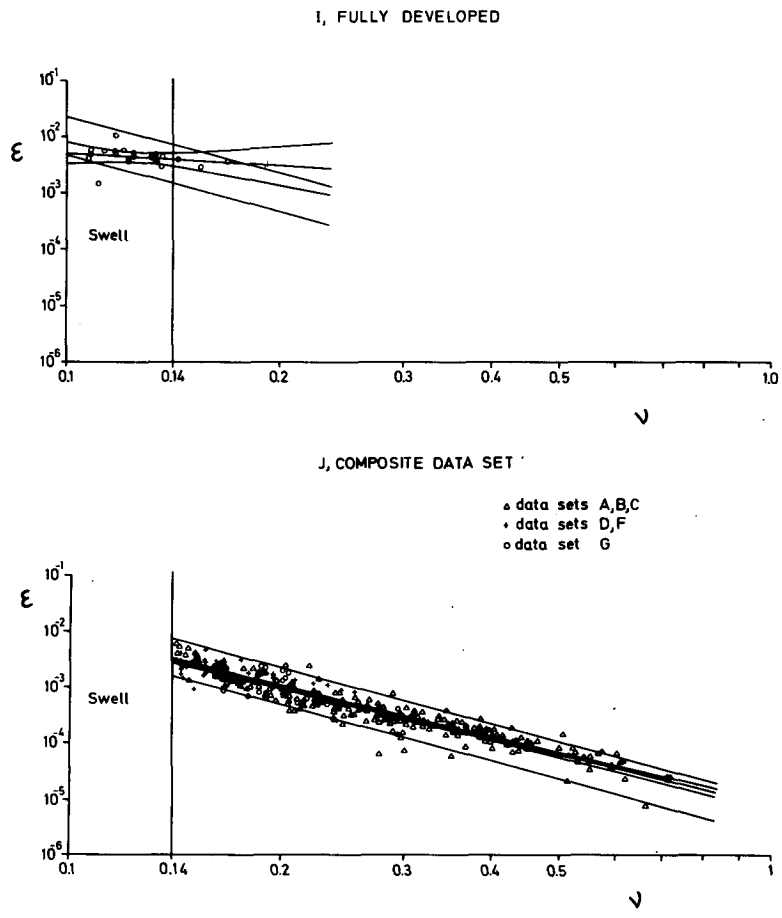

FIG. 10 ϵ-ν plots for the data sets A through J listed in Table 1. Notation as in Fig. 9.

deviation of a particular point from the regression line may also be regarded as the vertical distance that the regression line must be displaced in order to pass through the point. This corresponds to variations in the regression line constants $\log\alpha_0$ or $\log\epsilon_0$, which are plotted as ordinates in Figs. 11 and 12.

If all data sets could be regarded as selected randomly from a common data set, all error rectangles should lie in the vicinity of the rectangle for the composite data set J. This is clearly not the case. At the 95% confidence limit, which would be represented by rectangles approximately twice the size of the standard deviation rectangles, the rectangles for two out of six data sets in Fig. 11 and three out of six sets in Fig. 12 would fail to overlap with the composite set J. Thus it appears that there exist statistically significant differences between individual data sets, and therefore also statistically significant deviations of individual data sets from the equilibrium relations (6.1) and (6.2). However, a comparison of the standard deviations for each data set (and inspection of the actual data distributions in Figs. 9 and 10) suggests that these differences are immaterial in practice: the standard deviations for the individual data sets are not significantly lower than the standard deviation of the composite data set. For example, for the six data sets separately, the (unweighted) average standard deviation of $\log\alpha_0$ is 0.132, whereas for the composite data set the corresponding value is 0.168. The corresponding numbers for $\log\epsilon_0$ are almost identical—0.132 and 0.172, respectively. In terms of percentage variations of α_0 or ϵ_0, these values correspond to approximately 30% for the individual data sets and 40% for the composite data set. Thus for prediction purposes, the use of a common regression line [or the relations (6.1), (6.2), which lie close to the regression lines for J] is not significantly poorer than separate best-linear-fit relations for each data set.

The question then arises whether the scatter of the data is associated with the approximations of the one-parameter model and could be reduced by a more sophisticated treatment of the energy balance of the wave spectrum, or whether it originates in effects which cannot be included in any realistic numerical model and which must therefore simply be accepted as external noise.

In all data considered, the scales of the mean wind (eld were sufficiently large that the inequalities (7.4), fi7.5) were well satisfied. Thus the local-equilibrium ap-

proximation of the one-parameter model should have been applicable. That the (meso- and synoptic-scale) non-stationarity and inhomogeneity of the mean wind field cannot be the major cause for the observed scatter is also indicated by the significant variability of the JONSWAP data set A, which was selected with regard to high wind field uniformity. Inspection of individual JONSWAP generation cases suggests that the variability for this data set was probably due to small-scale gustiness of the wind field rather than hidden external parameters (J). A theoretical analysis indicated that wind field inhomogeneities in the 5–20 km length scale range could well have produced the observed effects.

The residual variability due to subgrid-scale wind field inhomogeneities may well represent a practical predictability limit for numerical wave forecasting and hindcasting. It would be of interest to pursue this question further with more sophisticated wave model studies including spectral shape parameters as free variables.

11. Conclusions

A simple wave model for growing seas has been proposed which is governed by a transport equation [(6.3)] for a single parameter $\nu = Uf_m/g$, where f_m is the peak frequency of the wave spectrum and U is the wind speed at 10 m height. The model is based on the premise that the response of the wave field to the wind input can be described by two processes which occur at different rates: 1) the rapid adjustment of the spectrum to a universal shape and an energy level such that the input by the wind in the central region of the spectrum is balanced by the nonlinear transfer (and, possibly, dissipation); and 2) the slower migration of the peak toward lower frequencies due to the nonlinear energy transfer across the peak.

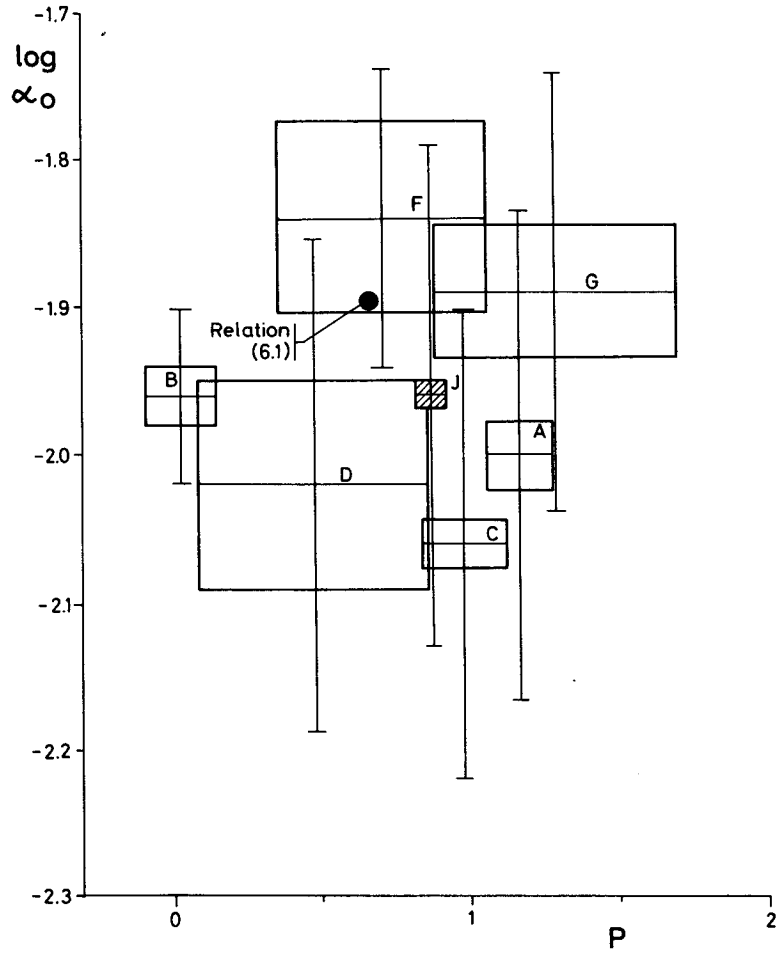

FIG. 11. Slopes r and constants $\log\alpha_0$ of the regression lines $\log\alpha = r(\log\nu - \log\nu_0) + \log\alpha_0$ [corresponding to the power law $\alpha = \alpha_0(\nu/\nu_0)^r$] for the data sets plotted in Fig. 9, excluding sets E, H and I. A fixed reference value $\log\nu_0 = -0.6$ is chosen for all data. Half-sides of rectangles represent standard deviations of p and $\log\alpha_0$. The 95% confidence limits are approximately twice as large. Error bars correspond to the standard deviations of the ordinates of individual data points from the regression line.

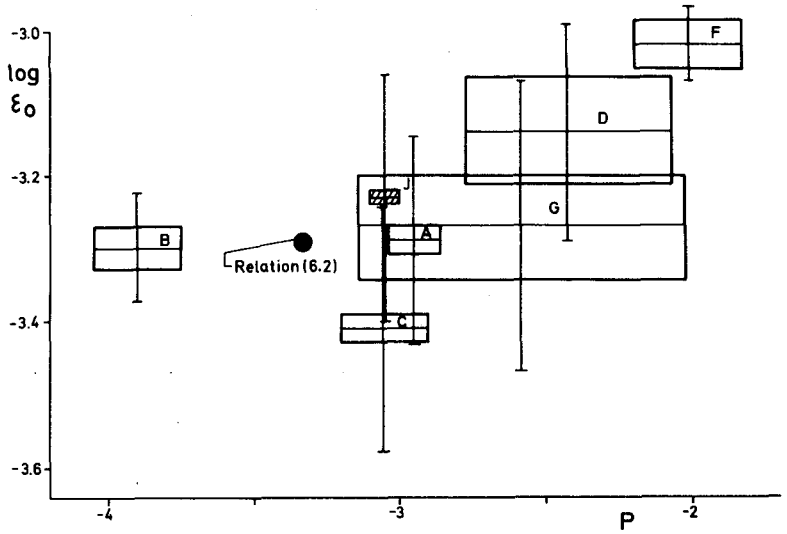

FIG. 12. Parameters r and $\log\epsilon_0$ of the regression line $\log\epsilon = r(\log\nu - \log\nu_0) + \log\epsilon_0$ [corresponding to the power law $\epsilon = \epsilon_0(\nu/\nu_0)^r$] for the data sets plotted in Fig. 10, excluding sets E, H and I. Notation as in Fig. 11.

The relaxation time of the first process is sufficiently small that the equilibrium can be regarded as essentially local. Thus the energy of the spectrum, characterized for example by Phillips' constant α, is a function of only the local wind speed and the frequency scale of the spectrum, determined by f_m. For dimensional reasons these parameters can occur only in the non-dimensional combination Uf_m/g. The quasi-equilibrium also applies to the angular distribution of wave energy in relation to the local wind direction, which must then be a universal function of the non-dimensional frequency f/f_m and ν. This leaves only a single free parameter ν to characterize the spectrum. The rate of change of ν, described by the transport equation (6.3), is an order of magnitude slower than the process responsible for the quasi-equilibrium, so that the position of the peak frequency represents a true integral response of the wave field to the entire wind field which must be determined in general by numerical integration of (6.3) under appropriate initial and boundary conditions.

Field measurements support the spectral shape invariance and energy-frequency relations (6.1), (6.2) on which the model is based. However, a test of the one-parameter transport equation (6.3) for more complex situations than the uniform-wind, limited-fetch cases against which it was calibrated is still lacking. This must await further wave measurements combined with detailed simultaneous documentation of the space-time structure of the generating wind field. Nevertheless, it is encouraging that the source terms in (6.3) determining the rate of migration of the peak could be derived rigorously from theory without adjustable constants. The only empirical input is the α-ν relation (6.1), which was tested against many different wind field cases.

The model is limited to growing seas and cannot be extended into the swell range. Swell represents the dynamically complementary situation to a growing wind sea in which to first order all wave components are decoupled and can be tracked independently along their propagation paths. Because of this decoupling, the swell limit is again mathematically tractable, but the appropriate numerical techniques for a swell model (characteristic mapping) are not immediately compatible with the parametric approach.

A complete wave model would probably need to use both representations in different parameter ranges. Apart from its usefulness for extensive wave climate computations, a simple combined model could be developed at a considerable savings in computer time over existing spectral techniques and would be ideally adapted to global wave forecasting, should the current efforts to obtain surface wind and wave data from satellites ultimately lead to an operating global system.

In conclusion, it may be mentioned that the energy balance relations (6.1), (6.2) on which the wave model is based may also have useful applications in the interpretation of remote sensing data itself. Although techniques have been proposed for the measurement of the full two-dimensional wave spectrum from space (cf. Ruck *et al.*, 1972), the tested simpler methods yield information on only a few parameters of the sea surface. For example, the average return pulse shape of nadir-looking short-pulse radar altimeters contains information on the rms wave height. The angular dependence of radar backscatter cross sections near vertical incidence can be used to determine the rms wave slope, and the cross sections for larger incidence angles yield the energy level of the spectrum in the centimeter–decimeter wavelength range. For a given spectral shape, these quantities can be related to ϵ, α and U, and with

the aid of relations (6.1) and (6.2) one can then recover both the surface wind and the wave spectrum.

REFERENCES

Barnett, T. P., 1968: On the generation, dissipation and prediction of ocean wind waves. *J. Geophys. Res.*, **73**, 513–530.

——, and J. C. Wilkerson, 1967: On the generation of ocean wind waves as inferred from airborne radar measurements of fetch-limited spectra. *J. Marine Res.*, **25**, 292–328.

Cardone, V. J., 1969: Specification of the wind field distribution in the marine boundary layer for wave forecasting. Rept. TR 69-1, Geophys. Sci. Lab., New York University.

Chakrabarti, S. K., and R. H. Snider, 1974: Wave statistics for March 1968 North Atlantic storm. *J. Geophys. Res.*, **79**, 3449–3458.

DeLeonibus, P. S., L. S. Simpson and M. G. Mattie, 1974: Equilibrium range in wave spectra observed at an open-ocean tower. *J. Geophys. Res.*, **79**, 3041–3053.

Dobson, F. W., 1971: Measurements of atmospheric pressure on wind-generated sea waves. *J. Fluid Mech.*, **48**, 91–127.

Elliott, J. A., 1972: Microscale pressure fluctuations near waves being generated by the wind. *J. Fluid Mech.*, **54**, 427–448.

Ewing, J. A., 1971: A numerical wave prediction method for the North Atlantic Ocean. *Deut. Hydrogr. Z.*, **24**, 241–261.

Garrett, J., 1969: Some new observations on the equilibrium region of the wind wave spectrum. *J. Marine Res.*, **27**, 273–277.

Gelci, R., and E. Devillaz (1970): Le calcul numérique de l'état de la mer. *Houille Blanche*, **25**, 117.

——, H. Cazalé and J. Vassal, 1957: Prévision de la houle. La méthode des densités spectroangulaires. *Bull. Inform. Comitè Central Oceanogr. d'Étude Cotes*, **9**, 416–435.

Hasselmann, K., 1962: On the non-linear energy transfer in a gravity-wave spectrum. 1: General theory. *J. Fluid Mech.*, **12**, 481–500.

——, 1963a: On the non-linear energy transfer in a gravity-wave spectrum. 2: Conservation theorems, wave-particle correspondence, irreversibility. *J. Fluid Mech.*, **15**, 273–281.

——, 1963b: On the non-linear energy transfer in a gravity-wave spectrum. 3: Computation of the energy flux and swell-sea interaction for a Neumann spectrum. *J. Fluid Mech.*, **15**, 385–398.

——, 1971: On the mass and momentum transfer between short gravity waves and larger-scale motions. *J. Fluid Mech.*, **50**, 189–205.

——, 1974: On the spectral dissipation of ocean waves due to white-capping. *Bound.-Layer Meteor.*, **6**, 107–127.

——, T. P. Barnett, E. Bouws, H. Carlson, D. E. Cartwright, K. Enke, J. A. Ewing, H. Gienapp, D. E. Hasselmann, P. Kruseman, A. Meerburg, P. Müller, D. J. Olbers, K. Richter, W. Sell and H. Walden, 1973: Measurements of wind-wave growth and swell decay during the Joint North Sea Wave Project (JONSWAP). *Deut. Hydrogr. Z.*, Suppl. A, **8**, No. 12.

Jenkins, G. M., and D. G. Watts, 1969: *Spectral Analysis and its Applications*. San Francisco, Holden-Day, 525 pp. (see pp. 109–110.)

Kitaigorodskii, S. A., 1961: Applications of the theory of similarity to the analysis of wind-generated wave motion as a stochastic process. *Izv. Akad. Nauk SSSR, Ser. Geofiz.*, No. 1, 73–80.

Liu, P. C., 1971: Normalized and equilibrium spectra of wind waves in Lake Michigan. *J. Phys. Oceanogr.*, **1**, 249–257.

Longuet-Higgins, M. S., and R. W. Stewart, 1964: Radiation stress in water waves, a physical discussion with applications. *Deep-Sea Res.*, **11**, 529–562.

Manasseri, R. J., 1967: The use of the Kolmogorov-Smirnov test to determine the existence of a fully developed sea (part 1). The mean spectrum for a fully developed sea recorded at Argus Island (part 2). Informal Rept. No. 67-36, Naval Oceanogr. Office, Washington D. C.

Mitsuyasu, H., 1966: Interaction between water waves and winds (I). *Rept. Res. Inst. Appl. Mech., Kyushu Univ.*, No. 14, 67–89.

——, 1968: On the growth of the spectrum of wind-generated waves. 1. *Rept. Res. Inst. Appl. Mech., Kyushu Univ.*, No. 16, 459–465.

——, 1969: On the growth of the spectrum of wind-generated waves. 2. *Rept. Res. Inst. Appl. Mech., Kyushu Univ.*, No. 17, 235–243.

——, 1973: The one-dimensional wave spectra at limited fetch. *Rept. Res. Inst. Appl. Mech., Kyushu Univ.*, No. 20, 37–53.

——, A. Tasai, T. Suhara, S. Mizuno, M. Ohkusu, T. Honda and K. Rikiishi, 1973: Studies on techniques for ocean wave measurements (2). *Bull. Res. Inst. Appl. Mech., Kyushu Univ.*, No. 40, 295–329.

——, ——, ——, ——, ——, —— and —— 1975: Observations of the directional spectrum of ocean waves using a cloverleaf buoy. *J. Phys. Oceanogr.*, **5**, 750–760.

Moskowitz, L., 1963: Estimates of the power spectra for fully developed seas for wind speeds of 20 to 40 knots. Tech. Rept., Navy Oceanogr. Office Contract N62306-1042, New York University, School of Engineering and Science.

——, W. J. Pierson, Jr., and E. Mehr, 1962: Wave spectra estimated from wave records obtained by the *OWS Weather Explorer* and the *OWS Weather Reporter* (I). Tech. Rept., Navy Oceanogr. Office Contract N62306-1042, New York University, School of Engineering and Science.

——, —— and ——, 1963: Wave spectra estimated from wave records obtained by the *OWS Weather Explorer* and the *OWS Weather Reporter* (II), Tech. Rept., Navy Oceanogr. Office Contract N62306-1042, New York University, School of Engineering and Science.

Patterson, M. M., 1974: Oceanographic data from Hurricane Camille. *Proc. Offshore Technology Conf.*, OTC 2109.

Phillips, O. M., 1963: On the attenuation of long gravity waves by short breaking waves. *J. Fluid Mech.*, **16**, 321–332.

Pickett, R. L., 1962: A series of wave power spectra. Informal manuscript report, No. 0-65-62, Naval Oceanogr. Off., 111 pp.

Pierson, W. J., Jr., and L. Moskowitz, 1964: A proposed spectral form for fully developed wind seas based on the similarity theory of S. A. Kitaigorodskii. *J. Geophys. Res.*, **69**, 5181–5190.

——, L. J. Tick and L. Baer, 1966: Computer based procedure for preparing global wave forecasts and wind field analysis capable of using wave data obtained from a spacecraft. *Proc. Sixth Symposium on Naval Hydrodynamics*, Washington, D. C., 499 pp.

Reece, A. M., and O. H. Shemdin, 1974: Modulation of capillary waves by long waves. *Proc. Symposium on Ocean Wave Measurement and Analysis*, ASCE, New Orleans, La.

Ross, D. B., V. J. Cardone and J. W. Conaway, 1970: Laser and microwave observations of sea-surface conditions for fetch-limited 17- to 25-m/s winds. *IEEE Trans. Geosci. Electron.*, **GE-8**, 326–335.

——, and ——, 1974: Observations of oceanic white caps and their relation to remote measurements of surface wind speed. *J. Geophys. Res.*, **79**, 444–452.

Ruck, G., D. Barrick and T. Kalisvewski, 1972: Bistatic radar sea state monitoring. Battelle Tech. Rept., Columbia Labortories, Columbus, Ohio.

Schule, J. J., L. S. Simpson and P. S. DeLeonibus, 1971: A study of fetch-limited wave spectra with an airborne laser. *J. Geophys. Res.*, **76**, 4160–4171.

Sell, W., and K. Hasselmann, 1972: Computations of nonlinear energy transfer for JONSWAP and empirical wind wave spectra. Unpubl. Ms., Inst. Geophys., University of Hamburg.

Snider, R. H., and Chakrabarti, 1973: High wave conditions ob-

served over the North Atlantic in March 1968. *J. Geophys. Res.*, **78**, 8793–8807.

Snodgrass, F. E., G. W. Groves, K. F. Hasselmann, G. R. Miller, W. H. Munk and W. H. Powers, 1966: Propagation of ocean swell across the Pacific. *Phil. Trans. Roy. Soc. London*, **A259**, 431–497.

Snyder, R. L., 1974; A field study of wave-induced pressure fluctuations above surface gravity waves. *J. Marine Res.*, **32**, 497–531.

——, and C. S. Cox, 1966: A field study of the wind generation of ocean waves. *J. Marine Res.*, **24**, 141–178.

Tyler, G. L., C. Teague, R. H. Stewart, A. M. Peterson, W. H. Munk and J. W. Joy, 1974: Wave directional spectra from synthetic aperture observations of radio scatter. *Deep-Sea Res.*, **21**, 989–1016.

Wilson, B. W., 1965: Numerical prediction of ocean waves in the North Atlantic for December 1959. *Deut. Hydrogr. Z.*, **18**, 114–130.